Mon. Not. R. Astron. Soc. **330,** 137–152 (2002)

Study of variable stars in the MOA data base: long-period red variables in the Large Magellanic Cloud

S. Noda,[1★] M. Takeuti,[2] F. Abe,[1] I. A. Bond,[3] R. J. Dodd,[3,4,13] J. B. Hearnshaw,[5] M. Honda,[6] M. Honma,[7] J. Jugaku,[8] S. Kabe,[9] Y. Kan-ya,[10] Y. Kato,[1] P. M. Kilmartin,[3,5] Y. Matsubara,[1] K. Masuda,[1] Y. Muraki,[1] T. Nakamura,[11] G. R. Nankivell,[4] C. Noguchi,[1] K. Ohnishi,[12] M. Reid,[13] N. J. Rattenbury,[3] To. Saito,[14] H. Sato,[11] M. Sekiguchi,[6] J. Skuljan,[5] D. J. Sullivan,[13] T. Sumi,[1] Y. Watase,[9] S. Wilkinson,[13] R. Yamada,[1] T. Yanagisawa,[1] P. C. M. Yock[3] and M. Yoshizawa[15]

[1]*Solar-Terrestrial Environment Laboratory, Nagoya University, Nagoya 464-8601, Japan*
[2]*Astronomical Institute, Tohoku University, Sendai 980-8578, Japan*
[3]*Dept. of Physics, University of Auckland, Auckland, New Zealand*
[4]*Carter National Observatory, PO Box 2909, Wellington, New Zealand*
[5]*Dept. of Physics and Astronomy, University of Canterbury, Christchurch, New Zealand*
[6]*Institute for Cosmic Ray Research, University of Tokyo, Kashiwa, 277-8582, Japan*
[7]*VERA Project Office, National Astronomical Observatory, 2-21-1 Osawa, Mitaka, Tokyo 181-8588, Japan*
[8]*Institute for Civilization, Tokai University, Japan*
[9]*High Energy Accelerator Research Organization (KEK), Tsukuba 305-0801, Japan*
[10]*Institute of Astronomy, University of Tokyo, Tokyo 181-0015, Japan*
[11]*Research Inst. Fundamental Physics, Kyoto University, Kyoto 606-8502, Japan*
[12]*Nagano National College of Technology, 381-8550, Japan*
[13]*School of Chemical and Physical Sciences, Victoria University, Wellington, New Zealand*
[14]*Tokyo Metropolitan College of Aeronautics, Tokyo 140-0011, Japan*
[15]*National Astronomical Observatory, Mitaka, Tokyo 181-8565, Japan*

Accepted 2001 October 15. Received 2001 October 15; in original form 2001 April 30

ABSTRACT

146 long-period red variable stars in the Large Magellanic Cloud (LMC) from the three-year Microlensing Observations in Astrophysics (MOA) project data base were analysed. A careful periodic analysis was performed on these stars and a catalogue of their magnitudes, colours, periods and amplitudes is presented. We convert our blue and red magnitudes to *K*-band values using 19 oxygen-rich stars. A group of red short-period stars separated from the Mira sequence has been found on a (log *P*,*K*) diagram. They are located at the short period side of the Mira sequence consistent with the work of Wood & Sebo. There are two interpretations for such stars; a difference in pulsation mode or a difference in chemical composition. We investigated the properties of these stars together with their colour, amplitude and periodicity. We conclude that they have small amplitudes and less regular variability. They are likely to be higher-mode pulsators. A large scatter has also been found on the long-period side of the (log *P*,*K*) diagram. This is possibly a systematic spread given that the blue band of our photometric system covers both standard *B* and *V* bands and affects carbon-rich stars.

Key words: catalogues – stars: AGB and post-AGB – stars: oscillations – stars: variables: other – Magellanic Clouds.

1 INTRODUCTION

There are many types of variable stars whose mechanism for variability (mainly pulsation, rotation, eruptive processes and geometric effects) is well studied and well understood observationally and theoretically. Among them, the pulsating variable stars have been investigated vigorously because they yield information on their stellar mass and their interior physical properties. They are a powerful tool for measuring distances in the Galaxy and extragalactic systems (1) because they are luminous and (2)

★E-mail: sachi@stelab.nagoya-u.ac.jp

because they have been shown empirically to obey a period–luminosity (PL) relation.

The PL relation for classical Cepheids was discovered by Leavitt (1908) and was used to measure the distance of galaxies. However, there is a discrepancy between the distance to the LMC derived from the PL relations for Cepheids and that derived for RR Lyraes (Walker 1992). This discrepancy may be due to uncertainties in the absolute calibration and a sensitivity to metallicity effects (Caputo 1997). It is important to establish PL relations of any new objects which are independent of these variable stars.

A PL relation for long-period red variables (Miras and semi-regular variables, hereafter SRs) will be a useful distance indicator because these stars are numerous and have high luminosities. However, they are the least-studied star type, because of their complex pulsation mechanism. Difficulties arise from uncertainties in our understanding of the convective energy transport and the opacity resulting from the many molecular absorption lines.

We present in this paper the results of our study of LMC Miras and SRs using the MOA data base. This data base was generated from the MOA project microlensing survey.

A PL relation for Miras of the Large Magellanic Cloud (LMC) was presented by Glass & Lloyd-Evans (1981) and Glass & Feast (1982). They observed 11 Miras in the infrared bands J, H and K. However, there was a large amount of scatter in the plot ($\sigma \sim 0.25$ mag) because their observation time was limited and it did not cover the whole phase of variations.

To reduce the scattering in the plot due to poor phase coverage, extensive infrared observations have been made (Feast et al. 1989; Hughes & Wood 1990), and a narrow PL relation was obtained ($\sigma \sim 0.13$ mag). Feast (1996) showed that the Miras in the LMC follow a narrow PL relation in both absolute bolometric magnitude, $M_{\rm bol}$, and absolute K-magnitude, M_K, and he concluded that all Miras pulsate in the same mode.

Wood & Sebo (1996) found two sequences in a K-band PL diagram for the small amplitude SRs in the LMC. One was the well-known Mira sequence, and the other (eight stars) was located at the position which is parallel to the Mira sequence and their periods were approximately half the periods of Miras on the PL diagram. This discovery encouraged a hypothesis that the pulsation mode of these stars in the secondary sequence must be in a higher mode. Using the *HIPPARCOS* data base of nearby stars, Bedding & Zijlstra (1998) discovered the SRs which are located in the secondary sequence of Wood & Sebo (1996). Bedding & Zijlstra interpreted the sequence of SRs as evolutionary (see Whitelock 1986).

Feast (1999) suggested that both Miras and SRs pulsate in the same mode, possibly both in the first overtone. The arguments were based on the angular diameter measurements of nearby Miras and the PL relationship of the Miras and SRs in globular clusters. He agreed with Bedding & Zijlstra (1998) that the sequence which is located on the shorter-period side of the Mira sequence in the PL plane is an evolutionary track ending at the Mira sequence. Feast also suggested that the Mira sequence would be a collection of variable stars with different chemical abundances and/or with different stellar mass. In this case, it was not necessary that Miras and SRs pulsate in different modes.

As described above, there are two theories on the short-period stars in the PL diagram for long-period red variable stars. Considering that the pulsation features of the Miras and SRs depend on several factors, other physical properties must also be considered. The study of stellar colour will be interesting because this gives us the temperature of stellar surface, stellar radius and mass which are the important factors of the pulsation period.

Recently, the continuous observation of a great number of stars using CCD cameras which cover a large image area became possible. The recent report of Wood (2000), based on the K-band photometry and the period derived from the MACHO data base indicated plausible sequences on the PL diagram. This diagram shows at least five sequences falling parallel to the Mira sequence. According to Wood, the three sequences containing the Mira sequence were explained as being different pulsation modes. However, more information is required to settle this issue. The features of the other two sequences are unknown, and it is expected that further independent observations and detailed investigation will reveal the nature of these stars.

We worked on the problem using the MOA data base which contained data for a large number of stars in the LMC. The period, magnitude colour, amplitude and periodicity for each star was determined.

We found an independent group of short period stars in a sample of 146 stars. We investigated the properties of these stars through their colour, amplitude and periodicity, and discuss the possibility of that they are higher mode pulsators.

Following an introduction to the MOA project, we describe our observation and photometry systems in Sections 2 and 3. To obtain the light curves of variable stars, a careful calibration of each image frame is required. This procedure is described in Section 4. In Sections 5 and 6, the data reduction and period analysis methods are described. In Section 7, the colour–magnitude diagram (CMD) of the LMC stars observed using our system is presented and the period-magnitude relation will be given in Section 8. The period–colour relation is presented and discussed in Section 9. The result of the conversion of MOA magnitudes to K-band values will be given in Section 10, along with a K, $\log P$ diagram. In Section 11 we discuss the possibility of the existence of multiple sequences in the $(\log P, K)$ plane with the amplitude distribution. In Section 12 we summarize our results.

2 THE MOA PROJECT OBSERVATIONS

2.1 Observational instruments

The MOA project commenced observations in May 1996 with the aim of observing microlensing events towards the LMC, SMC and Galactic bulge. The observational program was undertaken at the University of Canterbury's Mt. John Observatory (44°South, 1030 m above sea level) in the centre of the South Island of New Zealand.

The MOA project uses a 61-cm Ritchey–Chrétien Cassegrain telescope with modified optics to give a wide field of view (FOV) at $f/6.25$.

For the first set of observations in 1996 (Series 1), we used the original $f/13.5$ telescope optics and monitored $\sim 3 \times 10^5$ stars in three LMC fields with the mosaic CCD camera, MOA-cam1. MOA-cam1 was constructed with nine TI TC215 CCDs with 1000×1018 pixels; the pixel size was $12 \times 12\,\mu$m. From 1997 January to 1998 July, in Series 2, the optics were altered to $f/6.25$. MOA-cam1 covered three fields in the LMC bar (1×10^6 stars) and two fields in the SMC ($\sim 4 \times 10^5$ stars). The current set of observations, Series 3, started in 1998 August. For this series, a new camera, MOA-cam2 is in use. MOA-cam2 consists of three abutted SITe 2047×4095 pixel thinned, back-illuminated CCDs with $15 \times 15\,\mu$m pixels. The pixel size is 0.81 arcsec, giving a field

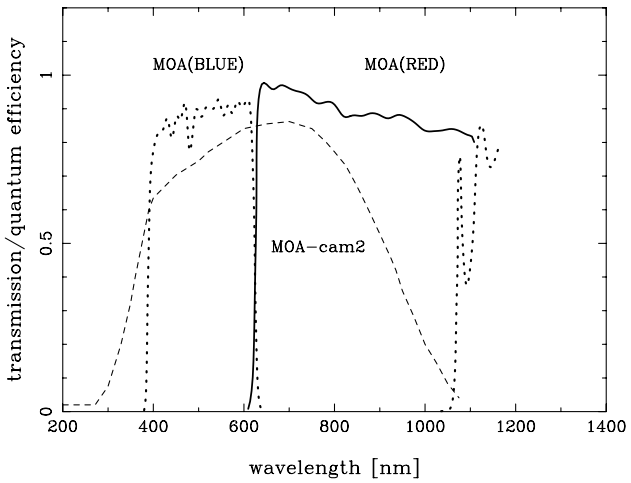

Figure 1. The transmission of the filters and quantum efficiency of MOA-cam2 are shown as a function of the wavelength. We used two broad-band filters (MOA_B, MOA_R), where MOA_B covers standard *B* and *V*, and MOA_R covers the Kron-Cousins *R*–*I* region.

of view of $0.5° \times 0.9°$ for each chip. The details of MOA-cam2 are in Yanagisawa et al. (2000). In this series we are observing 16 LMC fields (4.4×10^6 stars), eight SMC fields (9.3×10^5 stars) and 14 Galactic Bulge fields.

We used two broad-band filters to maximize photon collection. The MOA blue filter (MOA_B) covers 395–620 nm ($\lambda_{\rm eff} \sim 500$ nm) and MOA red filter (MOA_R) covers 620–1050 nm ($\lambda_{\rm eff} \sim 700$ nm). The spectral transmission curves for each filter are shown in Fig. 1.

The MOA instrumental photometry has been transformed to the standard Johnson *V* and Kron-Cousins *R* ($R_{\rm KC}$) by comparisons with about 100 stars imaged by the *Hubble Space Telescope* (*HST*). We describe these details in Section 4.

The variable star study based on the MOA data base was reported in Hearnshaw et al. (2000), Noda et al. (2000) and Takeuti et al. (2000).

2.2 Observation details

Regular 300-s exposures were made towards the LMC and the Small Magellanic Cloud. 180-s exposures were made for the Galactic bulge (GB) fields. Under the current system, it takes 70 s to read out the three CCD images for each exposure. Dark frames for each exposure were prepared every photometric night and dome flats or dark-sky flats were also frequently taken.

Observational data were archived on digital linear tape (DLT) tapes and all the data were analysed in both Japan and New Zealand. Series 1, 2 and 3 images were analysed using DOPHOT photometry software (Schechter, Mateo & Saha 1993). The size of the Series 2 data base created by the subsequent photometry is $\simeq$40 GB.

A new online analysis system based on image subtraction has been developed in New Zealand. In 2000 this system was able to find several microlensing events in real time and issue alerts to the astronomical community via the World Wide Web.[1] We are re-analysing some parts of our data with this method.

3 DATA ANALYSIS

Before undertaking data analysis using the DOPHOT program, all image files were prepared with the dark and flat-field frames. DOPHOT was used in a fixed position warm start mode, using the best photometric images as templates. It takes about 50 min to analyse one LMC frame with our computer. There were more than 400 measurements in the Series 2 (1.6 y) and Series 3 (1.4 y) data base. We obtain only relative magnitudes from the DOPHOT analysis. We also use non-standard filters, thus a transformation of our instrumental magnitude to the standard *V* and $R_{\rm KC}$ is required. This transformation is described in the next section.

4 CALIBRATION FOR MOA PHOTOMETRY

The transformation of the MOA photometry to the standard system was carried out using *HST* image data. More details are given by Kato (2000). We defined the transform relation for MOA-cam1 and MOA-cam2 separately because their CCD quantum efficiencies were quite different (the quantum efficiency of MOA-cam2 was twice as high as that for MOA-cam1). Although the filter system is exactly the same, this will cause serious differences in the relative magnitudes returned by DOPHOT. The DOPHOT magnitudes were calculated using photon quantities only, so a difference in CCD quantum efficiency will affect the DOPHOT output directly. To get standard magnitudes for MOA-cam2, we performed the procedure described below.

Photons coming from a star show a complicated scattering pattern around a central position caused by atmospheric turbulence. A point-spread function (PSF) models the scatter. The DOPHOT code estimated each magnitude using an elliptical Gaussian with seven free parameters as a model for a stellar PSF. A common PSF was adopted for all stars (bright stars and faint stars) in a frame, however it was clear that there were significant differences between the profiles for bright stars and that for faint stars. The former were weighted by the photon statistics of the star itself, and the latter were weighted by the photon statistics of the sky, so the latter should show larger scattering. The detailed study of the PSF indicated that the function often differs from the elliptical Gaussian (Alard & Lupton 1998). The error due to this discrepancy is approximately ± 0.05 mag for the bright stars and ± 0.09 mag for the faint stars. It was not a critical problem if we defined a mean magnitude with more than 100 measurement points to study stellar intensity, because the scatter due to PSF model inadequacy usually occurs at random.

As we were using large CCD chips, we have to determine the position dependent error for each CCD chip. In order to investigate this, we observed the globular cluster NGC 3201 at various positions on each chip, and compared stellar magnitudes with published magnitudes obtained using *B*, *V*, *R* and *I* filters by Alcaino, Liller & Alvarado (1989). We found that the error was smaller (± 0.015 mag) than the DOPHOT PSF photometry error ($\leq \pm 0.09$ mag). This was a systematic error however, and did not disappear even if we deal with a mean magnitude.

In the third step, also using the NGC3201 data, we computed the chip-to-chip differences for the magnitude zero point:

$$\mathrm{MOA}_{B(\mathrm{chip3})} = \mathrm{MOA}_{B(\mathrm{chip1})} - 0.23, \quad (1)$$

$$\mathrm{MOA}_{R(\mathrm{chip3})} = \mathrm{MOA}_{R(\mathrm{chip1})} - 0.31, \quad (2)$$

$$\mathrm{MOA}_{B(\mathrm{chip3})} = \mathrm{MOA}_{B(\mathrm{chip2})} - 0.34, \quad (3)$$

$$\mathrm{MOA}_{R(\mathrm{chip3})} = \mathrm{MOA}_{R(\mathrm{chip2})} - 0.41. \quad (4)$$

We used the chip3 scale as our standard as it gave the most linear response.

[1] http://www.phys.canterbury.ac.nz/ ~ physib/alert/alert.html

For the final step, we converted our MOA_B and MOA_R magnitudes to standard Johnson V and Kron–Cousins R (R_{KC}), respectively. The brightness of stars was acquired from an Analog Digital Unit (ADU; 1 ADU corresponded to 1.3 electrons for MOA-cam2) value which corresponded to the number of photons measured with the assumed PSF via the DOPHOT photometry. We define the zero-point of magnitude for MOA as 1 ADU. Therefore, all of the obtained magnitudes are negative, and we have to correct the zero-point of our magnitude in order to obtain actual magnitudes. We analysed the *HST* data of the LMC obtained with the Wide Field Planetary Camera2 (WFPC2) to correct for atmospheric seeing. As the filters for WFPC2 had been transformed to the Johnson V and R_{KC} by Holtzman et al. (1995), we were able to compare the converted HST magnitudes directly with those of our 100 stars.

Finally, we found a relation to convert the V_{m} and R_{m} for MOA-cam2;

$$V_{\mathrm{m}} = \mathrm{MOA}_B - 0.16(\pm0.01)(\mathrm{MOA}_B - \mathrm{MOA}_R) + 27.41(\pm0.01), \quad (5)$$

$$R_{\mathrm{m}} = \mathrm{MOA}_R + 0.29(\pm0.01)(\mathrm{MOA}_B - \mathrm{MOA}_R) + 27.24(\pm0.01), \quad (6)$$

$$\mathit{Colour}(V_{\mathrm{m}} - R_{\mathrm{m}}) = 0.53\mathit{Colour}(\mathrm{MOA}_B - \mathrm{MOA}_R) + 0.18. \quad (7)$$

For MOA-cam1;

$$V_{\mathrm{m}} = \mathrm{MOA}_B - 0.10(\pm0.01)(\mathrm{MOA}_B - \mathrm{MOA}_R) + 25.55(\pm0.01), \quad (8)$$

$$R_{\mathrm{m}} = \mathrm{MOA}_B + 0.31(\pm0.02)(\mathrm{MOA}_B - \mathrm{MOA}_R) + 25.45(\pm0.1), \quad (9)$$

$$\mathit{Colour}(V_{\mathrm{m}} - R_{\mathrm{m}}) = 0.59\mathit{Colour}(\mathrm{MOA}_B - \mathrm{MOA}_R) + 0.10. \quad (10)$$

Hereafter, we deal with V_{m} and R_{m} as the MOA standard magnitudes. In Fig. 2, we show the colour–magnitude diagram (CMD) obtained by MOA-cam2 for our observation fields in the LMC bar. The limiting magnitude was around 20.5 mag for MOA-cam2, and 19 mag for MOA-cam1. Because our passbands were broad and covered frequencies from violet to near infrared bands, the colour is not sensitive for blue stars.

To minimize the effects of the non-uniformity of the sky and system on the raw magnitudes (i.e. DOPHOT output magnitudes) we:

(i) divide the CCD chips into small regions (200×200 pixels),

(ii) select 80 bright stars which had more than 100 measurement points in each small region,

(iii) regard stars with a small scatter as 'non-variable' stars, i.e. where the number of observed points more than 4σ from the average magnitude was less than 15, and

(iv) calculate magnitudes for all stars by comparison with the 'non-variable' stars. That is, the MOA standard magnitudes were determined relative to the magnitudes of the near 'non-variable' stars in each small region.

Through the revision of our calibration procedure, we obtained progressive and interesting diagrams compared with our previous reports (Hearnshaw et al. 2000; Noda et al. 2000; Takeuti et al. 2000). Details are given in later sections.

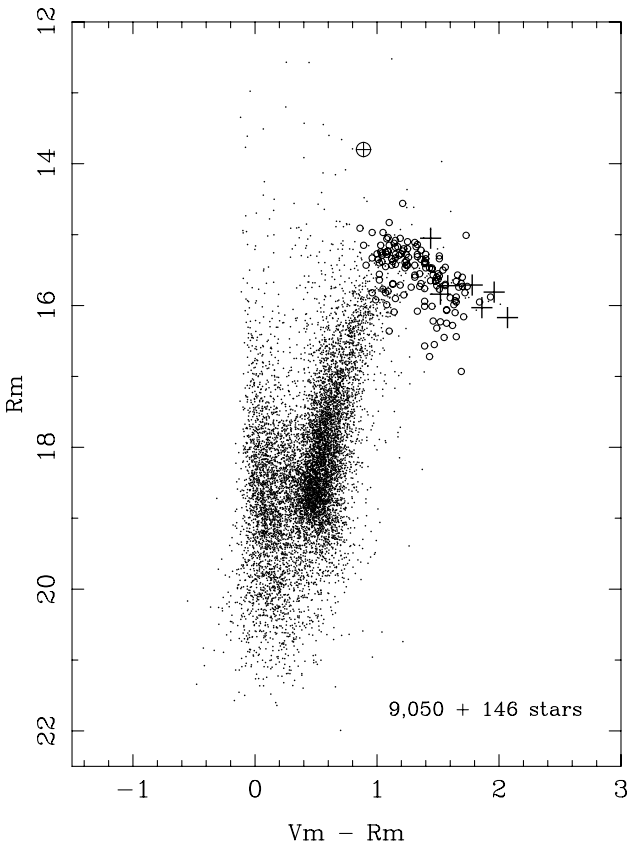

Figure 2. Colour–magnitude diagram (CMD) for the 146 stars in our sample with 9050 randomly chosen stars (dots). The vertical axis indicates R_{m}. All 146 stars are located on the tip of giant branch, which means they are in the AGB stage. The seven short period stars are indicated with + symbols. The ⊕ mark indicates nlmc3-214266 (see Section 7). The other stars are plotted as open circles.

5 DATA REDUCTION

We selected long-period red variables from the Series 2 data base using the following criteria

(i) Each star should be 'photometric' and have a 'single star shape' as judged by DOPHOT.

(ii) Light curves should be sufficiently long (≥ 100 points).

(iii) Light curves of each star must have large variability, i.e., the reduced χ^2 for a fit to mean brightness should be larger than $\chi^2_{Vm} \geq \chi^2_0$ and $\chi^2_{Rm} \geq \chi^2_0$. Here $\geq \chi^2_0$ corresponded to the upper 10 per cent limit of the reduced χ^2 distribution. For the MOA data base $\chi^2_0 = 4.3$.

To obtain large amplitude variables, we applied the additional following criteria.

(iv) Low-amplitude stars at an early stage of the study are rejected by removing those stars which had a magnitude difference between the fourth-highest and fourth-lowest magnitude values of less than 1.3 mag. This difference was larger than the amplitude δR_{m} determined in Section 6. This selection was carried out for the results of MOA-cam1 system without using the colour dependence in equations (8)–(10). This sample of large-amplitude stars might be affected when we use the correct colour relation.

(v) We select redder stars for large amplitude; $(V_{\mathrm{m}} - R_{\mathrm{m}}) \geq 0.4$ for the MOA-cam1 system.

We obtained 1067 light curves for the candidates of variable

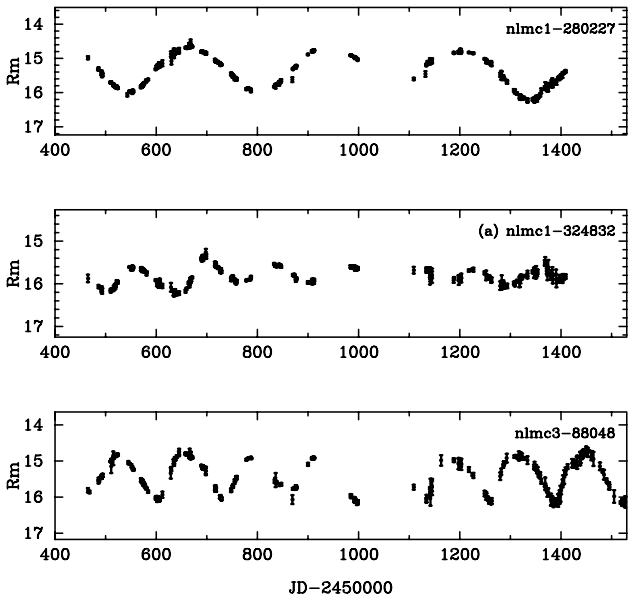

Figure 3. Examples of light curves for R_m. The periods for these stars were identified as 268.0, 133.5 and 131.2 d respectively, by the PDMM and PDM algorithms (see Section 6). The time axis spans from 1997 January to 1999 December. The error of each observation point is the DOPHOT PSF error. The stars nlmc1-324832 and nlmc3-88048 were a short-period red star and a short-period blue star discussed in Section 11. Lack of data after $JD = 2451400$ for nlmc1-280227 and nlmc1-324832 were due to instrumental problems with chip 1 on MOA-cam2.

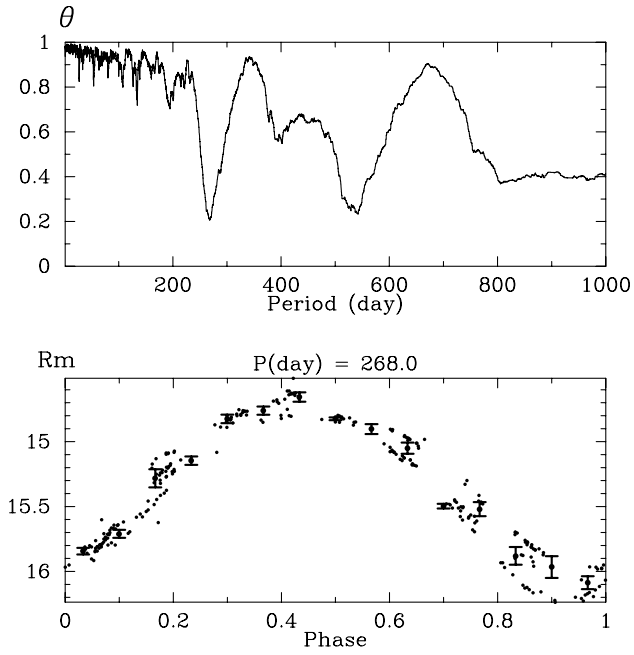

Figure 4. A sample of PDMM algorithm output for the same star, nlmc1-280227, as shown in Fig. 3. The top panel shows the reliability of period determination. θ is the sum of the dispersion of data in each bin for the given period. The period corresponding to the minimum of θ is chosen as the most likely period. The bottom panel shows the folded phase curve with the most likely period. The error bars indicate the standard deviation in each bin. The period of this star was determined as $P = 268.0$ d with $\theta = 0.21$.

stars with large amplitude after applying criteria (iv) and (v) on the Series 2 data base. Light curves from Series 2 and Series 3 were cross-referenced to stars from their respective templates. We rejected unreliable light curves, and finally obtained 908 light curves. In Fig. 3 we show an example of a light curve.

We also found 485 small-amplitude variable star candidates by applying a further criterion after numbers (i) to (iii) above. We analyse the large amplitude variables in this work. We will present the small amplitude variable star results in a future paper.

6 PERIOD ANALYSIS (PDMM)

As the first stage in the period analysis, we used the Phase Dispersion Minimization method for MOA (PDMM) which is a PDM method (Stellingwerf 1978) modified to operate on large photometry data sets. The PDMM algorithm finds a likely light-curve period together with a reliability parameter, θ, for a large number of light curves automatically. $\theta = 0$ indicates a complete cyclic change and $\theta = 1$ indicates no periodicity. The amplitude (the difference between the magnitudes of the brightest and the faintest bins) was also calculated. We converted the magnitudes of each bin to intensities and calculated the mean intensity. We denote the mean magnitude values as $\langle V_m \rangle$ and $\langle R_m \rangle$. We executed this code using both colours (V_m, R_m) for the 908 selected light curves.

Because our dataset included scattered data points, the PDMM algorithm sometimes gave integral multiples or sub-multiples of the period, or in the worst case, an incorrect result. To avoid simple errors in the periods obtained by the automatic analysis, we checked all code output carefully, and ran the PDM code manually to determine the most likely periods. We accepted a period which had good agreement between both colours. In Fig. 4, we present an example of PDMM figures. The upper diagram shows the reliability of the testing period. A small value of θ indicates a likely value for the period. The bottom diagram shows the light curve folded with the most likely period.

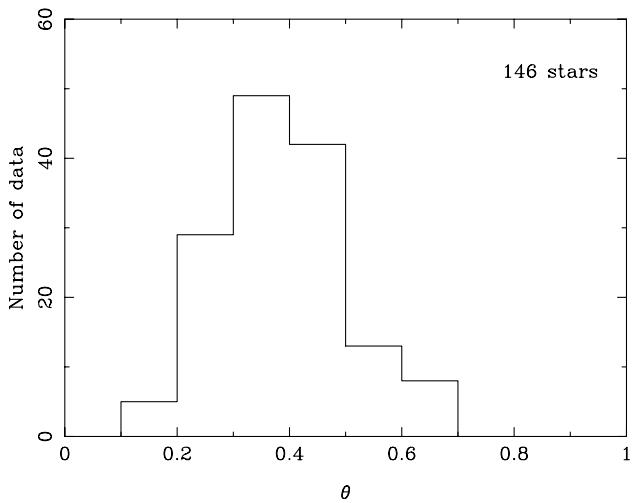

Figure 5. The distribution of θ calculated with 15 bins in PDMM. The mean of θ is approximately 0.38 for the 146 samples.

The total dataset (Series 2 to Series 3) extends over about 3 y ($\sim$1060 d), so periods less than $\sim$400 d should be well determined, because these have more than 2.5 cycles of variation within the observation period. We classified 908 candidate light curves by their features of periodicity. Among 908 stars, 329 stars show clear variability and of these, 259 stars had periods which were relatively well-determined. We rejected light curves such as eclipsing binaries, then chose light curves whose periods were longer than $\log P \geq 1.5$ (30 d). We also required $\log P \leq 2.6$ (400 d), reflecting

Table 1. 146 selected long-period red variables.

MOA ID	α (2000.0)	δ (2000.0)	$\langle R_m \rangle$	$\langle V_m \rangle$	δR_m	δV_m	Period [d]	θ	Remarks
nlmc1-108973	5:08:35.03	−69:14:58.03	15.43	16.34	0.85	1.09	111.3	0.38	
nlmc1-218899	5:08:42.78	−69:27:37.88	15.05	16.24	2.21	3.40	225.9	0.38	0509030-693121 (M)
nlmc1-109043	5:08:48.65	−69:07:36.64	15.66	17.14	1.82	2.34	360.0	0.20	
nlmc1-324832	5:09:21.74	−69:45:34.53	15.81	17.77	0.68	0.94	133.5	0.54	(a)
nlmc1-49182	5:09:21.78	−69:01:00.58	15.12	16.26	2.40	3.62	189.7	0.23	0509382-690440 (M6)
nlmc1-49228	5:09:37.02	−69:04:33.08	15.35	16.71	1.67	1.97	390.1	0.47	
nlmc1-324861	5:10:02.53	−69:53:24.67	15.08	16.23	0.97	1.36	203.8	0.30	
nlmc1-38733	5:10:19.99	−68:58:56.25	15.69	17.05	1.58	1.97	318.2	0.20	
nlmc1-153108	5:10:32.44	−69:22:05.18	15.56	16.58	1.12	1.49	120.3	0.43	
nlmc1-210097	5:10:45.58	−69:29:18.99	15.17	16.49	2.37	3.48	214.5	0.42	0511063-693253 (M)
nlmc1-316927	5:10:59.42	−69:52:08.58	15.40	16.80	2.06	2.83	237.8	0.20	
nlmc1-99040	5:11:01.50	−69:10:34.26	15.06	16.14	2.23	3.46	172.8	0.26	0511195-691408 (M)
nlmc1-38993	5:11:06.04	−68:57:43.41	16.57	17.96	0.66	0.85	136.2	0.45	
nlmc1-38583	5:11:23.97	−68:58:42.12	15.24	16.27	1.25	1.70	156.8	0.37	
nlmc1-316935	5:11:26.65	−69:45:47.39	15.43	16.74	1.02	1.24	225.6	0.41	
nlmc1-265052	5:11:28.31	−69:37:48.71	15.82	16.89	1.48	2.13	233.4	0.57	
nlmc1-264981	5:11:28.64	−69:35:31.69	15.55	17.05	1.21	1.62	313.1	0.29	
nlmc1-38559	5:11:42.14	−68:54:56.73	15.71	16.90	1.83	1.74	174.5	0.37	0511580-685826 (M)
nlmc1-98891	5:11:42.67	−69:15:01.51	15.27	16.47	2.48	3.76	186.2	0.33	0512015-691831 (M)
nlmc1-145336	5:12:12.00	−69:23:11.61	15.93	17.57	0.80	1.31	392.8	0.30	
nlmc1-200272	5:12:17.34	−69:30:27.11	14.97	15.93	1.50	1.96	200.8	0.25	0512385-693356 (M)
nlmc1-29759	5:12:20.50	−68:58:37.04	15.69	16.82	1.95	2.84	120.4	0.52	0512369-690204 (M)
nlmc1-88732	5:12:32.79	−69:07:54.10	15.92	16.91	0.59	0.85	373.1	0.52	
nlmc1-29858	5:12:54.21	−68:57:28.94	15.10	16.35	1.18	1.44	304.4	0.27	
nlmc1-200302	5:13:14.12	−69:29:30.26	15.28	16.36	1.26	1.71	155.3	0.44	
nlmc1-145125	5:13:16.04	−69:16:38.43	15.23	16.32	1.02	1.38	159.4	0.38	
nlmc1-145271	5:13:21.76	−69:19:55.66	15.66	17.31	1.08	1.50	338.8	0.30	
nlmc1-29756	5:13:24.80	−68:57:00.50	15.63	17.13	1.38	1.79	329.5	0.39	
nlmc1-200450	5:13:41.55	−69:29:36.64	16.23	17.75	1.75	2.39	370.2	0.47	
nlmc1-29775	5:13:48.12	−69:02:14.16	15.43	16.68	1.71	1.95	327.9	0.62	
nlmc1-29830	5:13:48.61	−68:56:03.79	15.82	17.54	1.26	1.59	375.1	0.31	
nlmc1-78039	5:14:01.66	−69:06:48.05	14.91	15.77	1.12	1.46	114.9	0.37	
nlmc1-189979	5:14:16.14	−69:30:56.46	15.47	16.87	1.46	1.93	322.2	0.32	
nlmc1-134678	5:14:40.39	−69:16:23.20	15.65	17.13	1.37	1.37	331.5	0.36	
nlmc1-189793	5:14:58.35	−69:34:50.89	15.46	17.02	0.85	1.22	238.4	0.36	
nlmc1-19391	5:15:11.62	−68:59:34.56	15.57	16.88	0.91	1.11	181.7	0.36	0515286-690250 (M)
nlmc1-78061	5:15:16.81	−69:09:55.76	15.70	17.26	1.82	1.63	360.0	0.44	
nlmc1-248333	5:15:19.16	−69:44:05.37	16.08	17.41	1.68	2.49	300.9	0.18	
nlmc1-78391	5:15:26.81	−69:15:07.48	14.56	15.77	2.67	3.53	256.5	0.27	0515461-691822 (M)
nlmc1-189766	5:15:38.31	−69:32:27.34	15.72	17.21	1.61	2.17	203.0	0.46	
nlmc1-248471	5:15:38.71	−69:40:33.73	16.16	17.87	1.47	2.20	219.6	0.34	0516017-694346 (M)
nlmc1-68195	5:16:06.44	−69:14:11.00	15.15	16.25	0.95	1.26	177.4	0.53	
nlmc1-239264	5:16:07.44	−69:44:25.89	15.05	16.49	1.38	2.21	129.5	0.34	(b)
nlmc1-68289	5:16:26.31	−69:06:26.52	16.09	17.23	1.39	1.76	106.8	0.38	
nlmc1-180512	5:16:28.90	−69:34:43.66	14.97	16.02	1.37	1.85	171.9	0.35	
nlmc1-10656	5:16:41.68	−68:58:50.43	15.42	16.57	1.10	1.46	166.5	0.40	
nlmc1-180542	5:16:57.23	−69:28:40.29	15.04	16.13	1.83	2.74	169.8	0.47	
nlmc1-239222	5:17:00.56	−69:37:04.13	15.57	17.23	1.47	1.59	230.4	0.48	
nlmc1-180614	5:17:25.95	−69:32:50.35	15.29	16.33	1.71	2.07	231.4	0.35	0517478-693554 (C)
nlmc1-58105	5:17:36.15	−69:10:28.62	15.28	16.68	2.31	2.80	254.1	0.21	0517551-691335 (M)
nlmc1-118904	5:17:50.20	−69:19:29.71	15.84	17.36	0.69	0.90	114.6	0.66	(c)
nlmc1-118910	5:18:09.10	−69:19:41.38	16.72	18.15	1.51	1.66	329.5	0.61	
nlmc1-228015	5:18:12.46	−69:37:48.46	15.70	16.83	1.50	1.89	127.8	0.46	0518353-694048 (M6)
nlmc1-280227	5:18:14.92	−69:52:10.99	15.29	16.47	1.56	1.86	268.0	0.21	0518400-695513 (C)
nlmc1-58139	5:19:02.89	−69:11:29.82	15.73	17.08	1.76	1.79	323.7	0.67	
nlmc1-228620	5:19:19.20	−69:37:28.60	16.93	18.62	1.36	2.04	218.2	0.52	
nlmc2-189096	5:19:19.29	−69:41:13.12	15.23	16.44	1.72	2.62	178.4	0.33	
nlmc1-170484	5:19:27.72	−69:33:31.21	15.27	16.27	1.06	1.39	127.1	0.44	0519502-693627 (M6)
nlmc2-120429	5:19:27.99	−69:35:12.11	15.15	16.04	1.62	2.19	200.9	0.42	
nlmc2-52704	5:19:45.24	−69:15:53.34	15.38	16.42	1.01	1.28	122.0	0.36	
nlmc2-189099	5:19:53.23	−69:41:17.89	15.43	16.55	1.28	1.74	155.9	0.44	
nlmc2-177924	5:20:19.80	−69:42:56.70	15.55	16.90	1.73	2.24	290.1	0.31	0520437-694548 (C)
nlmc2-107253	5:20:20.13	−69:33:44.89	15.32	16.58	1.43	1.82	326.0	0.23	0520427-693637 (C)
nlmc2-41103	5:20:36.32	−69:23:36.23	15.82	16.78	1.17	1.55	109.1	0.35	
nlmc2-242429	5:21:05.81	−69:54:12.77	15.71	17.49	0.69	1.17	116.9	0.45	(e)
nlmc2-177433	5:21:21.60	−69:38:19.96	15.77	17.28	1.46	2.21	360.3	0.40	0521450-694107 (C)
nlmc2-242076	5:21:39.38	−69:51:48.16	15.72	17.30	0.81	1.20	100.0	0.45	(d)
nlmc2-242294	5:21:54.42	−69:50:23.21	15.80	16.89	1.47	2.14	110.5	0.36	
nlmc2-300067	5:21:59.83	−69:55:53.71	15.40	16.42	1.49	1.94	147.6	0.47	
nlmc2-166505	5:22:26.69	−69:37:40.10	16.36	17.46	0.98	1.13	86.3	0.44	
nlmc2-300177	5:22:34.06	−69:56:21.38	15.28	16.61	1.08	1.36	304.0	0.28	0523006-695904 (C)

Table 1 – *continued*

MOA ID	α (2000.0)	δ (2000.0)	$\langle R_m \rangle$	$\langle V_m \rangle$	δR_m	δV_m	Period [d]	θ	Remarks
nlmc2-95318	5:22:44.35	−69:33:44.04	15.47	16.92	1.25	1.61	349.6	0.62	0523078-693626 (C)
nlmc2-29822	5:22:47.09	−69:24:09.76	15.47	16.90	1.31	1.76	291.2	0.30	
nlmc2-165804	5:22:50.36	−69:36:04.41	15.18	16.33	1.12	1.44	259.4	0.36	
nlmc2-29809	5:22:58.41	−69:22:05.02	15.17	16.34	0.77	0.97	207.1	0.50	
nlmc2-300086	5:23:01.57	−69:59:54.20	15.14	16.47	1.70	2.31	344.3	0.18	0523288-700234 (C)
nlmc2-166417	5:23:01.76	−69:36:33.08	15.90	17.05	2.50	3.61	113.1	0.53	
nlmc2-95223	5:23:08.01	−69:26:18.59	15.57	17.03	1.07	1.32	374.4	0.41	
nlmc2-95219	5:23:22.49	−69:25:59.77	14.83	15.93	1.32	1.64	256.4	0.39	
nlmc2-300087	5:23:35.11	−69:59:59.44	15.34	16.74	1.27	1.62	321.7	0.28	0524023-700237 (C)
nlmc2-95417	5:23:50.06	−69:26:59.64	16.25	17.82	1.46	1.61	365.7	0.32	
nlmc2-289306	5:23:54.19	−70:02:21.75	16.06	17.63	1.26	1.56	212.9	0.30	
nlmc2-289270	5:24:03.14	−69:57:01.83	15.72	17.28	0.94	1.24	349.6	0.59	
nlmc2-84657	5:24:11.45	−69:31:22.34	15.64	16.66	1.28	1.70	130.0	0.30	
nlmc2-151799	5:24:33.90	−69:37:02.27	16.17	18.24	0.92	1.50	127.6	0.45	(f)
nlmc2-151839	5:24:41.01	−69:38:22.69	16.07	17.64	2.13	2.19	284.4	0.35	
nlmc2-19377	5:25:04.75	−69:19:37.68	16.03	17.89	0.73	0.99	121.1	0.40	(g)
nlmc2-220283	5:25:26.54	−69:52:41.04	15.45	16.52	1.18	1.66	136.0	0.29	
nlmc2-19266	5:25:27.46	−69:23:44.32	15.41	16.80	1.01	1.26	207.7	0.42	
nlmc2-19930	5:25:32.02	−69:24:09.81	16.44	18.09	1.15	1.81	161.0	0.28	0525543-692639 (M)
nlmc2-10220	5:25:44.68	−69:15:18.16	15.58	17.09	1.42	1.71	324.7	0.30	
nlmc2-143085	5:26:09.35	−69:38:20.30	15.20	16.45	1.77	2.65	210.8	0.33	
nlmc2-279164	5:26:40.45	−69:59:52.40	15.43	16.67	0.91	1.21	197.4	0.26	
nlmc2-74407	5:26:53.26	−69:29:16.22	15.25	16.32	1.19	1.50	145.3	0.33	
nlmc2-279125	5:26:58.78	−69:58:32.37	15.35	16.36	0.85	1.15	106.2	0.43	
nlmc2-210119	5:27:07.83	−69:47:20.33	15.38	16.77	1.73	2.38	326.7	0.41	
nlmc2-10255	5:27:15.64	−69:23:51.38	15.28	16.43	0.63	0.90	145.0	0.44	
nlmc2-64540	5:28:06.72	−69:32:27.26	15.31	16.64	1.28	1.78	211.3	0.30	0528300-693445 (CS)
nlmc2-133102	5:28:17.73	−69:42:02.80	15.73	17.47	0.60	1.14	203.2	0.47	
nlmc2-64521	5:28:33.77	−69:29:52.95	15.85	17.07	2.07	1.78	205.0	0.27	0528568-693208 (M)
nlmc3-315892	5:28:45.00	−70:22:53.81	15.24	16.33	0.89	1.21	168.7	0.34	0529167-702511 (M1)
nlmc3-88398	5:28:46.04	−69:48:34.53	16.01	17.46	1.32	1.73	244.1	0.37	
nlmc3-202382	5:28:50.33	−70:00:40.08	15.15	16.18	0.99	1.16	171.6	0.52	
nlmc2-266041	5:28:51.17	−70:00:40.45	15.10	16.16	1.00	1.14	155.4	0.54	
nlmc3-37184	5:28:54.49	−69:40:12.48	15.38	16.51	1.32	2.00	157.6	0.56	
nlmc3-202460	5:29:01.01	−70:06:46.74	15.65	17.09	1.65	1.53	395.5	0.46	0529303-700902 (C)
nlmc3-262474	5:29:09.79	−70:12:38.77	15.28	16.52	1.21	1.43	262.3	0.51	
nlmc3-144789	5:29:13.07	−69:50:42.18	15.50	17.04	1.22	1.67	355.6	0.43	
nlmc3-88237	5:29:17.03	−69:43:33.34	15.22	16.58	2.42	3.50	239.3	0.27	
nlmc3-37148	5:29:22.54	−69:36:11.89	15.89	17.49	1.58	2.30	209.9	0.29	0529467-693825 (MS)
nlmc3-37121	5:29:29.15	−69:32:51.15	15.34	16.46	1.92	2.95	172.6	0.30	
nlmc3-145171	5:29:40.22	−69:57:37.65	16.45	18.00	2.26	2.54	316.8	0.61	
nlmc3-144814	5:29:47.07	−69:53:24.80	15.60	17.09	0.92	1.32	195.1	0.49	
nlmc3-88048	5:29:52.38	−69:44:09.13	15.33	16.29	1.27	1.62	131.2	0.20	
nlmc3-37227	5:29:59.70	−69:31:41.76	15.95	17.79	0.70	1.13	264.6	0.64	
nlmc3-306907	5:30:01.02	−70:20:04.46	15.99	17.62	3.30	2.83	356.5	0.27	0530323-702216 (M6)
nlmc3-251030	5:30:17.43	−70:18:14.96	15.88	17.81	0.76	1.18	350.5	0.44	
nlmc3-306731	5:30:26.09	−70:22:50.30	15.99	17.07	1.41	1.60	231.1	0.22	
nlmc3-191203	5:31:22.09	−70:00:30.54	16.32	17.81	1.50	1.27	384.2	0.49	
nlmc3-77881	5:31:22.87	−69:46:29.21	15.20	16.42	1.04	1.42	287.7	0.26	
nlmc3-77928	5:31:28.35	−69:40:48.78	15.60	16.91	1.42	1.81	242.1	0.36	
nlmc3-306656	5:31:33.65	−70:27:53.96	15.77	16.82	1.70	2.51	111.1	0.40	0532066-703000 (M)
nlmc3-78091	5:31:53.61	−69:47:07.41	15.74	17.02	1.34	1.86	162.2	0.40	
nlmc3-18475	5:32:02.11	−69:34:59.72	15.73	17.43	1.00	1.53	257.8	0.37	
nlmc3-241225	5:32:02.93	−70:16:01.83	15.74	17.41	1.10	1.48	335.4	0.31	
nlmc3-18489	5:32:11.61	−69:35:45.07	15.11	16.42	2.44	3.50	246.0	0.19	
nlmc3-122522	5:33:24.88	−69:59:40.53	15.47	16.70	1.49	1.91	262.3	0.22	
nlmc3-179656	5:33:46.70	−70:06:52.06	16.01	17.40	1.37	1.52	357.5	0.48	
nlmc3-169613	5:34:09.26	−70:09:14.16	15.33	16.48	0.90	1.27	190.7	0.65	
nlmc3-10545	5:34:11.85	−69:38:20.19	15.60	17.30	0.92	1.19	261.8	0.41	
nlmc3-288613	5:35:04.46	−70:21:59.56	15.95	17.60	1.29	1.56	357.1	0.32	
nlmc3-288533	5:35:11.73	−70:22:43.25	15.88	17.53	1.40	1.59	307.6	0.41	0535442-702433 (C)
nlmc3-288854	5:35:15.43	−70:22:19.52	16.28	17.90	1.10	1.53	209.0	0.35	
nlmc3-222606	5:36:03.70	−70:13:43.72	15.49	16.94	1.43	1.79	301.9	0.29	0536347-701529 (C)
nlmc3-222499	5:36:25.59	−70:19:15.90	15.37	16.61	1.77	2.92	173.0	0.35	
nlmc3-4366	5:36:32.90	−69:31:50.43	15.94	17.33	1.02	1.34	135.4	0.50	
nlmc3-162051	5:36:44.15	−70:09:44.26	15.01	16.74	1.64	2.22	378.2	0.41	
nlmc3-54070	5:36:52.50	−69:48:14.15	15.69	17.38	0.70	1.31	235.6	0.41	0537193-694955 (MS)
nlmc3-280668	5:37:04.69	−70:26:27.05	15.30	16.81	1.88	2.78	238.2	0.27	
nlmc3-222737	5:37:05.26	−70:18:42.66	15.39	16.62	1.33	1.71	258.9	0.19	
nlmc3-272280	5:38:23.36	−70:23:32.55	16.22	17.68	1.48	1.96	342.2	0.18	
nlmc3-214306	5:38:25.79	−70:18:21.96	15.34	16.85	0.70	1.09	241.6	0.38	

Table 1 – *continued*

MOA ID	α (2000.0)	δ (2000.0)	$\langle R_m \rangle$	$\langle V_m \rangle$	δR_m	δV_m	Period [d]	θ	Remarks
nlmc3-214266	5:38:52.12	−70:18:56.05	13.80	14.69	0.84	1.22	113.4	0.38	(1)
nlmc3-214430	5:39:07.31	−70:17:05.09	15.76	17.15	1.31	1.66	299.6	0.20	
nlmc3-214415	5:39:16.10	−70:15:56.36	16.10	17.74	1.21	1.56	315.4	0.23	
nlmc3-272161	5:39:22.78	−70:22:27.14	15.26	16.30	1.56	2.32	129.0	0.35	
nlmc3-272613	5:39:27.49	−70:25:27.95	16.55	18.02	1.14	1.53	308.4	0.40	

Note: $\langle R_m \rangle$, $\langle V_m \rangle$ are the intensity mean magnitude of R_m or V_m respectively, and θ is the PDM algorithm reliability parameter. (a) ∼ (g) and (1) are the stars referred to in the text. Numbers in the 'Remarks' column are the identification number (with spectral type) in Hughes & Wood (1990).

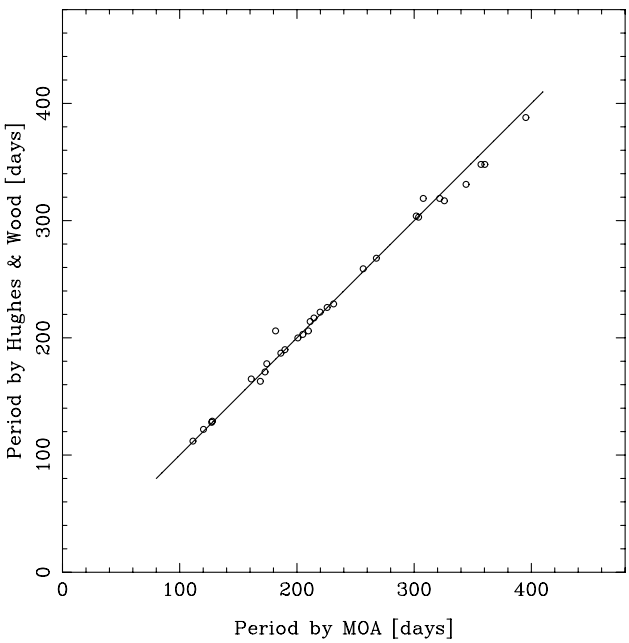

Figure 6. The comparison between the periods determined by our PDM (horizontal axis) and the period tabulated in Hughes & Wood (1990) (vertical axis). The differences are quite small (≤ 2 per cent).

the dataset time-span. Finally, 146 light curves were left. The reliability parameter θ for these curves is less than 0.67 (the mean ∼0.38) with 15 folding bins. We show the distribution of θ in Fig. 5.

Other candidates, the stars with poorly determined periods, short-periods or small amplitudes, will be the subject of future work. Here we give observational values for 146 stars in Table 1 (ID, α, δ, $\langle R_m \rangle$, $\langle V_m \rangle$, δR_m, δV_m, Period, θ). ID is the MOA data base star number and (α,δ) are the Right Ascension and Declination, respectively. Comparing the coordinates of 629 stars in tables 2–6 of Hughes & Wood (1990) with our sample, we identified at least 34 stars as a control. The ID numbers of their tables are indicated in the 'Remarks' column of Table 1. Spectral types given in the tables of Hughes & Wood are also shown. The 34 stars consisted of 21 oxygen-rich stars and 13 carbon-rich stars. In Fig. 6, we show the relation between the period determined via the PDM method and the period tabulated in Hughes & Wood (1990) for 30 stars whose periods are well-determined by us. It is clear that the periods are coincident and the differences between MOA and Hughes & Wood (1990) is less than 2 per cent. We used these 30 stars for the conversion to the *K*-magnitude system as described in the following section. Here, we note that Hughes & Wood (1990) tabulated two periods, 170-d and 319 d, for the star nlmc3-288533. We adopted 319 d as the period because we obtained 307.6 d for the period of this star via our analysis using the PDM method.

7 COLOUR–MAGNITUDE DIAGRAM (CMD)

Fig. 2 shows the distribution of our sample of 146 variable stars on a colour–magnitude diagram (CMD) with 9050 randomly chosen stars for reference. In this figure, the 146 stars were located at the tip of the giant branch. According to the stellar evolution theory, stars with initial mass of about 1–8 $M_\odot$ evolve into asymptotic giant branch (AGB) stars with carbon and oxygen cores. Although we only required a large variation in each light curve and restricted the colour condition and period in our selection criteria for variable stars (Section 6), these stars were located in one particular region in the CMD. Consequently we presumed that these stars form a group which were in a common evolutionary stage and pulsate by a common mechanism. However, there was an extremely bright star (indicated by a ⊕ mark) in this CMD, nlmc3-214266, which we have mentioned below. Also we will describe the seven stars with + marks in Section 11. nlmc3-214266 and these seven stars are denoted by (1) or (a)–(g) respectively in Table 1.

8 PERIOD–LUMINOSITY RELATION

We show a plot of $\langle V_m \rangle$ magnitude versus period in Fig. 7. Open circles indicate stars whose R_m amplitudes (δR_m) are smaller than 2.2 mag. Filled circles indicate the stars whose amplitude are larger than 2.2 mag. The line indicates the regression fit for the stars with $\log P \geq 2.2$;

$$\langle V_m \rangle = 2.01(\pm 0.43) \log P + 12.10(\pm 1.05). \quad (11)$$

The trend to be fainter in $\langle V_m \rangle$ has been known in previous studies. The star, which was extremely bright in the CMD, nlmc3-214266 ($\langle V_m \rangle = 14.69$, $\log P = 2.05$, ⊕ mark in Fig. 7), was also much brighter than the other stars with similar periods in this diagram. We also show the $(\log P, \langle R_m \rangle)$ plot in Fig. 8. The slope of this distribution for the stars with $\log P \geq 2.2$ was less than that in $(\langle V_m \rangle, \log P)$ plane but still had a downward tendency. The best-fitting line for these stars is;

$$\langle R_m \rangle = 1.13(\pm 0.33) \log P + 12.84(\pm 0.80) \quad (12)$$

The star, nlmc3-214266, was again quite bright ($\langle R_m \rangle = 13.80$) and was separate from the other samples. The scatter of the $\langle V_m \rangle$ magnitude ($\sigma \sim 0.52$) was larger than that of $\langle R_m \rangle$ ($\sigma \sim 0.39$), which was possibly due to the difference between oxygen-rich stars and carbon-rich stars. We will discuss this in Section 10.

9 PERIOD–COLOUR RELATION

We show the period–colour $(\log P, \langle V_m \rangle - \langle R_m \rangle)$ plot in Fig. 9.

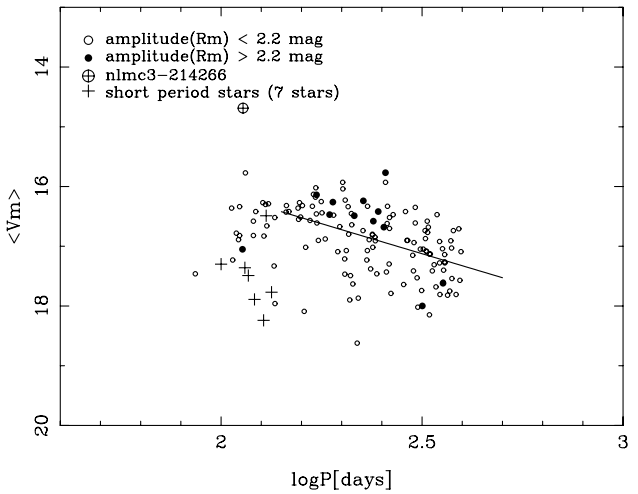

Figure 7. The period–magnitude ($\langle V_m \rangle$) diagram. Open circles are the stars whose amplitude (δR_m) are less than 2.2 mag. Filled circles are the stars whose amplitude are larger than 2.2 mag. The extremely bright star, nlmc3-214266, is indicated by the $\oplus$ mark. This star is much brighter than the other stars with similar period in this diagram. The cross-marks indicate the stars of group *B* (indicated in Section 11). The downward line indicates the least-squares fitting for the stars with $\log P \geq 2.2$.

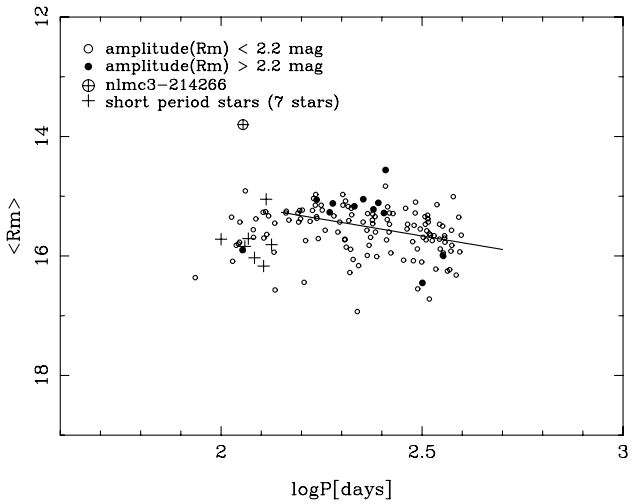

Figure 8. The period–magnitude ($\langle R_m \rangle$) diagram. See Fig. 7 for an explanation of the symbols used.

The upward line indicates the regression line for the stars with $\log P \geq 2.2$;

$$\langle V_m \rangle - \langle R_m \rangle = 0.88(\pm 0.16) \log P - 0.74(\pm 0.38) \qquad (13)$$

In this figure, the colour of most stars with longer periods ($\log P \geq 2.2$) were much redder than that of the short-period stars, and the relationship was more constrained ($\delta \sim 0.19$) compared with that shown in Figs 7 and 8.

9.1 nlmc3-214266

In Fig. 9, star nlmc3-214266 is positioned in the main group. When compared with the other stars of similar period (open and filled circles), the effective temperature of this star should be similar, as the colour ($\langle V_m \rangle - \langle R_m \rangle$) was almost equivalent. The brightness of nlmc3-214266 was high in both $\langle V_m \rangle$ and $\langle R_m \rangle$, therefore its radius

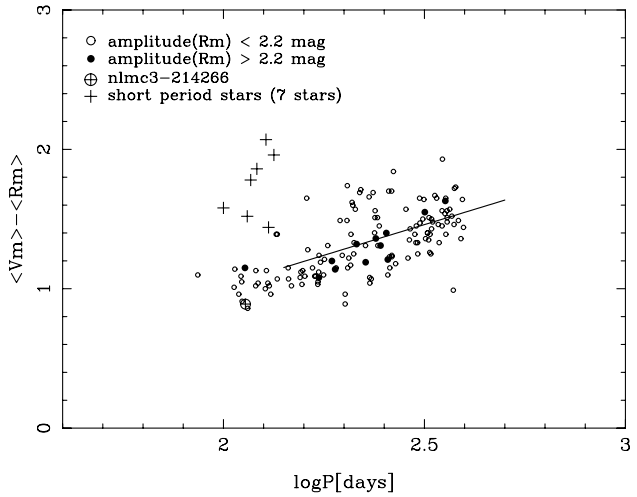

Figure 9. The period–colour ($\langle V_m \rangle - \langle R_m \rangle$) diagram. The relationship shows a narrower band compared with Figs 7 and 8. The seven stars with short period (+ symbols, see Section 11.2) show the extreme red colour, while nlmc3-214266 is not conspicuous (see Section 9.1).

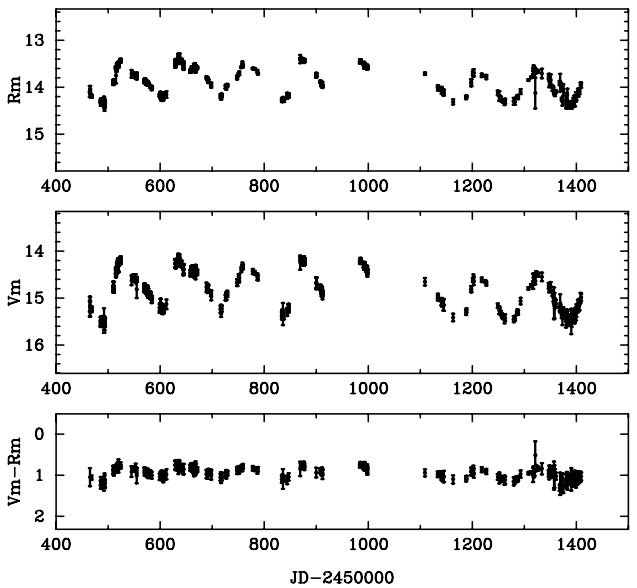

Figure 10. The light curve of nlmc3-214266. This star is quite bright in the period–magnitude diagrams (Figs 7 and 8), not red in the period–colour diagram (Fig. 9), and again bright in the ($\log P$,K_m) diagram (Fig. 15).

must have been large compared to the stars in the main group. The star was almost certainly HV 1011, which was a suspected Cepheid (Kurochkin 1992). Kurochkin was unable to obtain a period for this star and our results do not conclusively suggest that this star is a classical Cepheid. When the pulsation period is the same, a larger star must have a higher mass considering the relation between the period and the mean density of stars. Therefore we assumed that nlmc3-214266 was a massive star evolved from the main sequence, and not an AGB star. The light curve is presented in Fig. 10. The star nlmc3-214266 was a luminous semi-regular variable. In the Galaxy, V810 Centauri is one of the variable stars which is more luminous and has a higher temperature than the AGB in the CMD. Kienzle et al. (1998) estimated that the spectral type of this star was F8 Ia, the period was approximately 156 d, $M_{bol} = -8.5$, and the

initial mass was $\sim 25\,M_{\odot}$. Such a heavy star will become a supernova rather than a AGB star (e.g. Becker 1998).

9.2 Short-period red stars

In Fig. 9, several stars whose periods were $\log(P/d) < 2.15$ were distributed towards the red region and were separated from the main group of stars. If the colours are different between stars with a similar period and luminosity, their mass or pulsation property ($Q = P\sqrt{\bar{\rho}}$) should be different. It is quite important to investigate their luminosity because the relation between luminosity and colour gives information about their radius, i.e. mass and pulsation parameter (Q) of each star. Although our $\langle V_{\rm m}\rangle$ and $\langle R_{\rm m}\rangle$ are trustworthy they cover too small a wavelength range to enable the energy distribution of such red stars to be discussed directly. Therefore, we study the relationship between our magnitudes and the near-infrared (near-IR) luminosity in Section 10.

9.3 nlmc1-239264

We note that there were no data points for the minima of the light curve for nlmc1-239264. Therefore the mean magnitudes, $\langle V_{\rm m}\rangle$ and $\langle R_{\rm m}\rangle$, for this star were calculated by using only the bright phases. This just gives the brighter limit of the mean magnitude for this star. Regarding the period, we assumed that the determined period for the star ($P = 129.5$ d, or $\log P = 2.11$) was accurate because there were three maxima in the light curve. On Figs 7 and 8, the star was located near the extension of the least squares fitted line for stars with $\log P \geq 2.2$. When we used a dataset covering complete cycles, the stars were located at fainter positions. We used $\langle V_{\rm m}\rangle - \langle R_{\rm m}\rangle = 1.44$ as the blue or lower limit of the colour average in Fig. 9. The star was located about half a magnitude redder than the least-squares-fitted line in Fig. 9. Considering the incompleteness of our dataset, we may assume that the star nlmc1-239264 should be located at a fainter position on Figs 7 and 8, and at a redder or higher position on Fig. 9.

9.4 nlmc3-306907

The star, nlmc3-306907, is the remarkable star because of its unique colour ($\langle V_{\rm m}\rangle - \langle R_{\rm m}\rangle$) variation, i.e. the colour was bluer when $\langle V_{\rm m}\rangle$ and $\langle R_{\rm m}\rangle$ were fainter. The light variation is shown in Fig. 11. Among 146 samples, nlmc2-151839 and nlmc3-191203 also showed the same property, though to a lesser extent. The colour variations of all the other stars were fainter when the $\langle V_{\rm m}\rangle$ and $\langle R_{\rm m}\rangle$ were brighter, which is a common feature of radial pulsators. Such an extraordinary property might indicate the development of a particular molecular band caused by a different chemical composition in the stellar surface.

10 PERIOD TO *K*-MAGNITUDE RELATION

It is well known that Miras fall on a narrow PL sequence on the ($\log P$,K) plane (Feast et al. 1989; Hughes & Wood 1990). Wood & Sebo (1996) discovered a second sequence located on the short-period side of Miras, while Bedding & Zijlstra (1998) found strong evidence that semi-regulars (SRs) near the Sun's position in the ($\log P$, K) plane lie in a region which coincides with the second sequence found by Wood & Sebo (1996). Also, the existence of at least two (or four) sequences other than Miras was indicated from the analysis of MACHO data base (Wood 2000).

The K-band ($\sim 2.2\,\mu$m) corresponds closely to the maximum

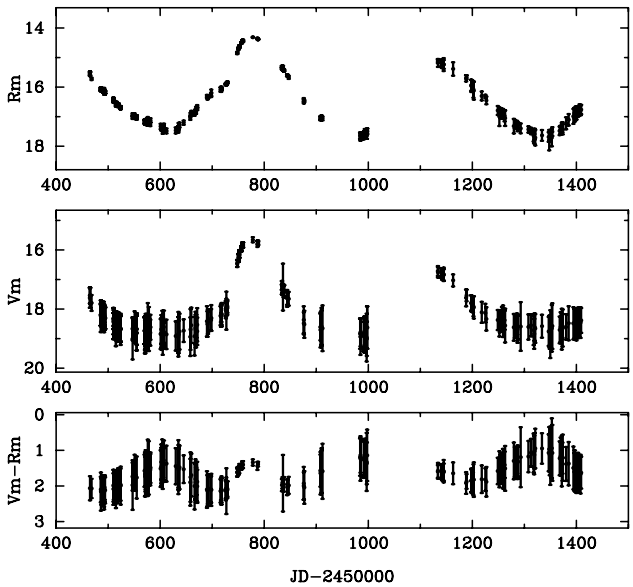

Figure 11. The light curve of nlmc3-306907. The colour ($\langle V_{\rm m}\rangle - \langle R_{\rm m}\rangle$) is bluer when the $\langle R_{\rm m}\rangle$ and $\langle V_{\rm m}\rangle$ are fainter.

radiation flux of long-period red variables, so that the discrepancy between K-magnitudes and bolometric magnitudes should be relatively small. Because previous studies have been performed with K-magnitudes, we have to convert our observational magnitude $\langle V_{\rm m}\rangle$, $\langle R_{\rm m}\rangle$ into K-magnitudes in order to compare our results with the established PL relation.

First, to define our conversion scale, we identified 34 stars which were the same as those published by Hughes & Wood (1990) from our 146 sampled long-period red variable stars (see Section 6). The 34 identified stars consisted of 21 oxygen-rich (M-type) stars and 13 carbon-rich (C-type) stars. Furthermore, we selected 19 oxygen-rich stars whose periods were well-determined in our analysis, and used them to calibrate our $V_{\rm m}$,$R_{\rm m}$ magnitudes to K values;

$$\langle R_{\rm m}\rangle - K_{\rm shv} = 2.10(\langle V_{\rm m}\rangle - \langle R_{\rm m}\rangle) + 1.22. \quad (14)$$

$K_{\rm shv}$ was the K-magnitude tabulated in Hughes & Wood (1990) (*shv* is the prefix of the star number). Hereafter we write $K_{\rm m}$ in place of $K_{\rm shv}$ as our custom K-magnitude. We discuss here a few reasons for the scatter ($\sigma \sim 0.15$ mag) in this relation. First, and possibly most importantly, the K-magnitudes obtained by Hughes & Wood (1990) were determined with only a single observation, whilst we were dealing with the average magnitudes of at least 100 measured points. Although amplitudes of long-period red variable stars are large (~ 0.6 mag) in the K band, a single epoch observation provides the magnitudes on the various phase of light variations, so it should have caused extra scattering in our $K_{\rm m}$ conversion. Secondly, our transformed magnitudes ($V_{\rm m}$ and $R_{\rm m}$) which were obtained with our broad-band filters do not correspond to a standard V or $R_{\rm KC}$ (also K) exactly. Finally, as mentioned in Section 4, there was an uncertainty of approximately ± 0.015 mag dependent on the image position on each CCD chip. The result from comparing the K-magnitudes of Hughes & Wood (1990) and the average MOA magnitudes had a similar scatter to that due to the intrinsic variability of the stars. We also calculated the probable K-magnitudes by extrapolating the observed light curves backwards to the time of observation of Hughes & Wood (1990). The scatter found in this case was larger and most probably due to the

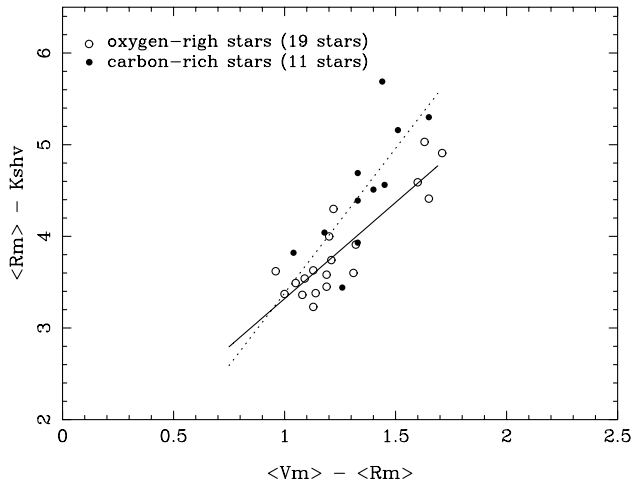

Figure 12. Comparison of $(\langle R_m\rangle - K_{shv})$ and the MOA Colour $(\langle V_m\rangle - \langle R_m\rangle)$. K_{shv} is the magnitude as tabulated in Hughes & Wood (1990). Open circles indicate the oxygen-rich stars and filled circles indicate the carbon-rich stars. The solid line indicates the K_m conversion formula (14), while the dashed line indicates the least squares fitting for the 11 carbon-rich stars (formula 15). The solid line makes a good fit to the oxygen-rich stars, while the 11 carbon-rich stars fall on the another steeper (dashed) line.

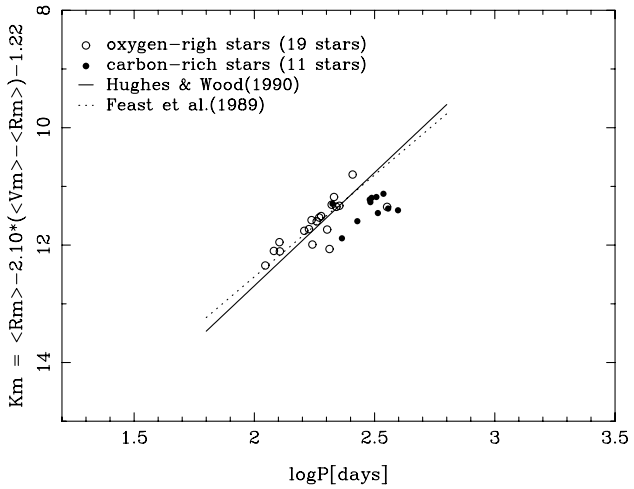

Figure 13. K_{shv}-magnitude versus period for 19 oxygen-rich stars and 11 carbon-rich stars which were identified with Hughes & Wood (1990) as the same stars. The lines are the O-Mira sequences obtained by previous studies (Feast et al. 1989; Hughes & Wood 1990).

imperfect periodicity of Mira variables. As the resulting relation was nearly the same as equation (14), that expression was used in the following study.

Now we estimated the coincidence of our K_m conversion with formula (14). In Fig. 12, we show a $(\langle V_m\rangle - \langle R_m\rangle, \langle R_m\rangle - K_{shv})$ plot for 19 oxygen-rich stars (open circles) and 11 carbon-rich stars (filled circles) which were common in Hughes & Wood (1990) and our catalogue, and show the well-determined periods by our analysis. 19 oxygen-rich stars were used to derive formula (14) which is indicated by the solid line. It is obvious that the conversion formula (14) fits the oxygen-rich Miras (O-Miras) ($\sigma \sim 0.15$ mag) well but does not fit the carbon-rich stars ($\sigma \sim 0.34$ mag). The dashed line indicates another conversion formula using 11 carbon-rich stars:

$$\langle R_m\rangle - K_{shv} = 3.16(\langle V_m\rangle - \langle R_m\rangle) + 0.22. \quad (15)$$

We also show the $(\log P, K_m)$ diagram for these 19 oxygen-rich stars and 11 carbon-rich stars in Fig. 13. The two lines in this figure were the sequences of O-Miras from previous studies (Feast et al. 1989; Hughes & Wood 1990). Our converted magnitudes K_m for 19 oxygen-rich stars agreed well with these classical relations ($\sigma \sim 0.18$ mag). In contrast, those for 11 carbon-rich stars appear below the lines ($\sigma \sim 0.25$ mag). According to the results from previous observations, the PL relation for O-Miras and carbon-rich Miras (C-Miras) are similar in the K band (Feast et al. 1989). In Figs 12 and 13, we conclude that our conversion formula (14) makes a good enough fit to the oxygen-rich stars, but does not fit to the carbon-rich stars.

We consider here why such a disagreement arises for the carbon-rich stars. As is well known, there are roughly two kinds of spectral types, M and C, for long-period variable stars depending on the relative abundance of oxygen to carbon in their atmospheres. This causes a remarkable difference in colour tendency (Smak 1964). The B-band (V_m-magnitude in this paper) flux of oxygen-rich (M-type) stars was smaller than that for carbon-rich (C-type) stars. This was due to the existence of some strong TiO bands resulting from their rich abundance of oxygen. Therefore, carbon-rich stars are bluer than oxygen-rich stars at the same effective temperature, which means that the value of $(\langle R_m\rangle - K_{shv})$ for carbon-rich stars, is greater than that for oxygen-rich stars even if the colour index $(\langle V_m\rangle - \langle R_m\rangle)$ is the same (see Fig. 12). This explains why the K-magnitudes for carbon-rich stars were less luminous in Fig. 13, when we derived the conversion scale, K_m, using only oxygen-rich stars.

The above results were derived from the data by Hughes & Wood (1990). Within these stars (21 O-Miras and 13 C-Miras), the K-magnitudes of nlmc3-306907 and nlmc3-288533 were reported in table 4 of Trams, van Loon & Waters (1999). The former is an oxygen-rich star and the latter is a carbon-rich star. Their results are shown in Table 2.

Peak-to-peak modulation was found in the light curve of nlmc3-288533. The magnitudes tabulated in Table 2 were brighter than $\langle K_m\rangle$, 11.35 and 11.20, of each star. The differences of magnitudes at the light maxima and $\langle K_m\rangle$ were 1.00 and 0.55 mag respectively. Such differences can be accepted as the light variations of this type of variable stars.

When we adopt the K-magnitude by Trams et al.(1999), K_T, in Fig. 12, the position of nlmc3-306907 moves upward and seems to belong to the carbon-rich stars. However, this star should not be regarded as a typical oxygen-rich star because of the unusual colour variation it showed, as mentioned in Section 9.4. The position of nlmc3-288533 in Fig. 12 will be slightly lower than the current position.

Fig. 14 shows a similar diagram using the K-magnitude (K_S: $\sim 2.15\,\mu$m) of the DENIS catalogue (http://cdsweb.u-strasbg.fr/denis.html). Among 146 samples, 139 stars have been found, and K-magnitudes were given for 119 stars in the DENIS catalogue. The correlation between K_S and K_m is given by the equation,

$$K_S = 0.9(\pm 0.09)K_m + 0.73(\pm 1.07), \quad (16)$$

with a standard deviation of 0.47. Such a scatter may be explained as the results of intrinsic light variability. In Fig. 14, oxygen-rich and carbon-rich stars were located in the lower and the upper regions, as seen in Fig. 12. The star nlmc3-306907 was again located in the carbon-rich star region. No K_S data for nlmc3-288533 has been found. If nlmc3-306907 is a typical

Table 2. *K*-magnitudes reported by other observations.

Star	JD	*K*/mag	Sources	Remarks
nlmc3-306907	2446341	10.96	Hughes &Wood (1990)	phase ≈ 0.8
	2450788	10.35	Trams et al. (1999)	near a light maximum
nlmc3-288533	2446341	10.58	Hughes & Wood (1990)	phase ≈ 0.8
	2450782	10.65	Trams et al. (1999)	near a light maximum

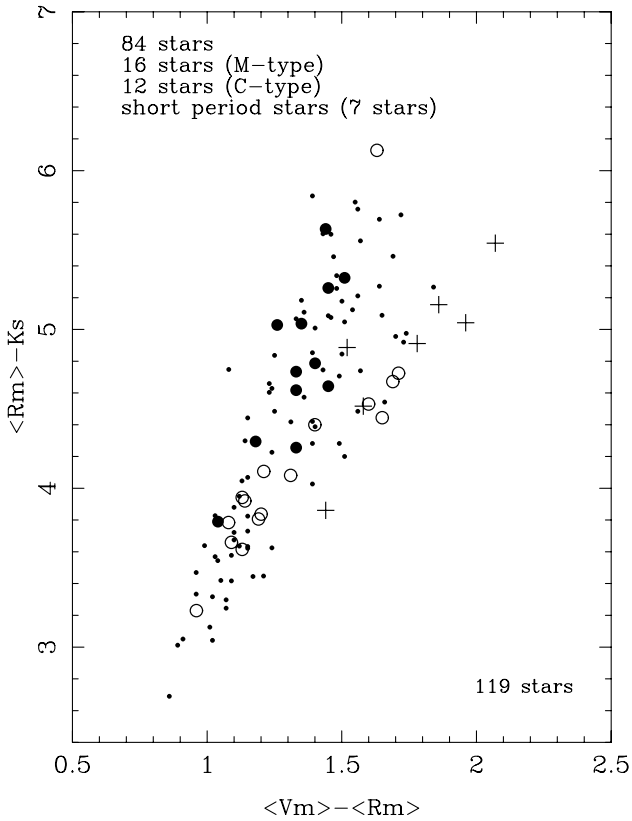

Figure 14. The $(\langle V_m\rangle - \langle R_m\rangle, \langle R_m\rangle - K_S)$ relation for identified 119 stars. K_S indicates the *K*-magnitude from the DENIS catalogue (see text).

oxygen-rich star, this indicates that some oxygen-rich stars may exist at the upper side of the oxygen-rich relation in Fig. 12. Therefore, brighter oxygen-rich stars than given by equation (14) may exist.

We show a $(\log P, K_m)$ diagram for our sample of 146 stars in Fig. 15. In this figure, the solid diagonal line is the LMC PL relation for O-Miras of Hughes & Wood (1990) and the dotted line shows the track for O-Miras of Feast et al. (1989). Three groups, designated *A*, *B* and *C* are evident in Fig. 15. They are discussed in detail in Section 11. The stars in the most populous group lie close to these lines. nlmc3-306907 is located in the same region as carbon-rich stars. Another star, nlmc2-64521, is also located below the established relation. Therefore it is clearly hard to decide the all star below these lines are carbon-rich stars.

One of the 13 carbon-rich stars, nlmc2-64540, lies on these lines as an exception, and the remaining 12 carbon-rich stars fall below these lines. The slope of K_{shv} magnitude versus MOA Colour (see Fig. 12 and formula 15) for carbon-rich stars is steeper than that for oxygen-rich stars, so these lines intersect. This was why this exceptional carbon-rich star was located near the line of formula (14) and lies on the sequences for O-Miras in Fig. 15 (also in Fig. 13).

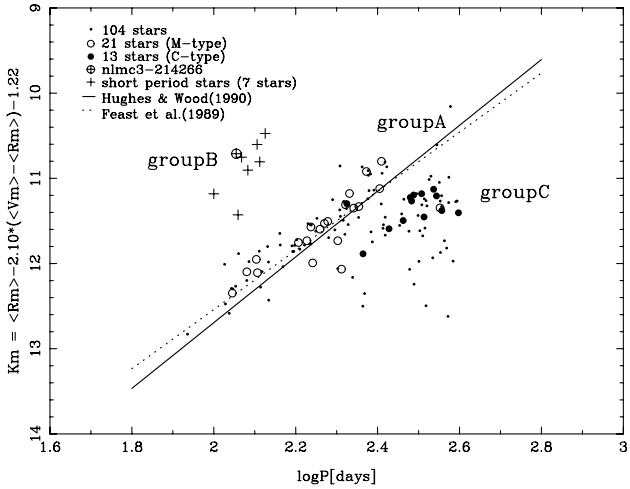

Figure 15. The $(\log P, K_m)$ diagram for 146 long-period red variable stars. Two lines are the $(\log P, K)$ relations for O-Mira sequences by the previous studies. The stars in the most populous group of our samples lie on the O-Mira sequence. One exceptional carbon-rich star also lies on the O-Mira sequence, while most of carbon-rich stars fall below these sequences. The + marks (seven samples) indicate the noteworthy stars with short period, and the ⊕ indicates nlmc3-214266 (see text). An explanation of groups *A*, *B* and *C* is given in the text.

We note that it was possible that at least ∼50–60 carbon-rich stars were included in the sample of 146 stars because the ratio of oxygen-rich (the sample of 21 stars) and carbon-rich (the sample of 13 stars) stars was approximately ∼62 and ∼38 per cent respectively. These could generate the extra scatter in the $(\log P, K_m)$ plot.

When we converted the MOA data into *K*-magnitudes by using equation (15), most of the stars, including 11 carbon-rich stars (around group *C* in Fig. 15), were found near the empirical LMC PL relation for C-Miras, but some of them remained in the fainter domain of the diagram. The isolation of the short period variable stars (seven '+' mark stars and a '⊕' star, defined in the next section) became clearer in this case.

11 DISCUSSION

11.1 $\log P$–K_m diagram

It is difficult to estimate *K*-magnitudes from the large photometry data base as it was originally designed to detect microlensing events. However, we have now succeeded in estimating *K*-magnitudes using the properties of oxygen and carbon-rich stars as described in the previous section. Based on these results, we can investigate the $(\log P, K_m)$ diagram more carefully.

As described in Section 10, our conversion of $\langle V_m\rangle$ and $\langle R_m\rangle$ into K_m magnitude could not be applied for carbon-rich stars, and they are located below the main sequence of Figs 13 and 15. Therefore the scatter in the $(\log P, K_m)$ plane (Fig. 15) must be associated with

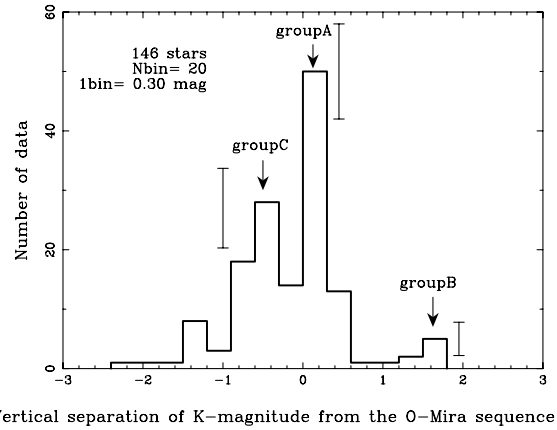

Figure 16. The histogram of the vertical distance of *K*-magnitude from the O-Mira sequence of Hughes & Wood (1990) in Fig. 15. The 146 star sample is used. The highest peak at $\delta K = 0$ contains stars agreeing with the Mira ($\log P$, K) relation by Hughes & Wood (1990). We classified these stars as group *A*. The stars separated by $\sim +1.5$ mag from group *A* were defined as group *B*. The stars separated by ~ -0.6 mag were defined as group *C* (see text). The error bars beside each group are described in the text.

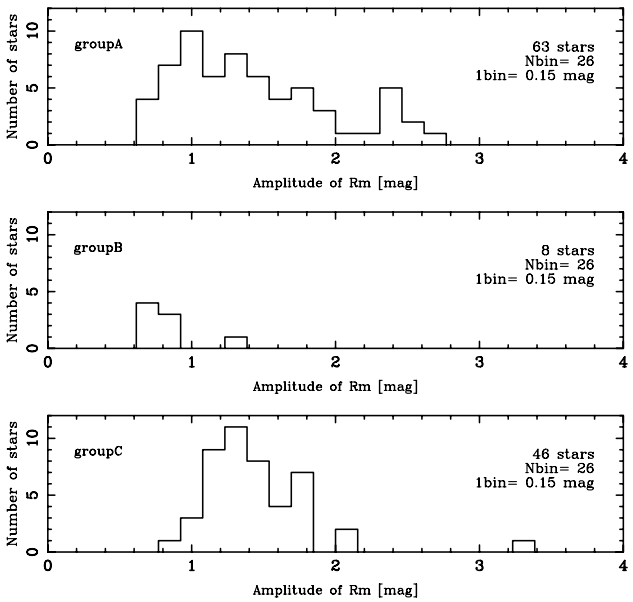

Figure 17. The distributions of pulsation amplitude in R_m for each group. The upper panel shows stars on the most populous sequence (i.e., group *A*). The middle panel shows the distribution for the stars in group *B* which were located on the shorter period side of group *A*. The bottom panel shows that for the stars in the group *C* sequence which were located on the longer period side of group *A*.

these stars. However, even taking the above fact into account, the scatter in the plot is too large to be described by one sequence. To demonstrate this point, in Fig. 16 we show a histogram of vertical distance from the line of O-Mira sequence by Hughes & Wood (1990):

$$K = -3.86(\log P - 2.4) + 11.5 \qquad (17)$$

The error bars are equal to the square root of the number of stars in each of the three groups identified in Fig. 16.

A vertical separation of zero means it was on the Hughes & Wood (1990) track in Fig. 15. The most populous group, *A*, lies at

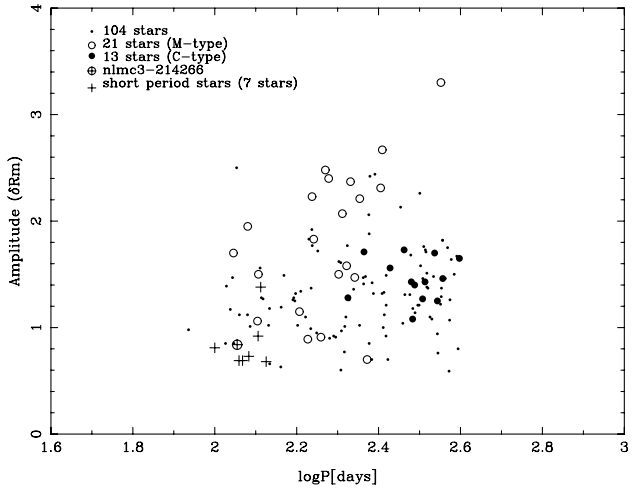

Figure 18. The period−amplitude (δR_m) diagram. The symbols are the same as Fig. 15. Group *B* stars have been found in the low-amplitude domain.

this position. This group contained the stars with largest amplitude. There was a small peak (group *B*, eight stars) around $+1.5$ mag (corresponding to a leftward shift in period in Fig. 15). The group *B* stars are relatively small amplitude variables. Another peak that is relatively broad can be identified at around -0.6 mag (group *C*, corresponding to a rightward shift in period in Fig. 15). We define each group in Fig. 16 using the following limits: the stars distributed between 0 and 0.6 mag as group *A*, the stars distributed greater than 0.9 mag are as group *B*, and stars distributed between -0.9 and -0.3 mag as group *C*.

In Fig. 17 we show the amplitude distribution, δR_m for the stars in each group. In Fig. 18 we show the ($\log P$, δR_m) diagram with the same symbols as Fig. 15. In Fig. 17, it is clear that most of largest amplitude ($\delta R_m \geq 2.2$ mag) variable stars are group *A* stars, which provides strong proof that these stars are Miras.

In contrast, the amplitudes of stars in group *B* were smaller ($\delta R_m \leq 1.4$ mag) than most of the others as shown in Fig. 17 and Fig. 18. This group includes the seven short-period stars and nlmc3-214266. This group is located on the very short period side ($\log P \leq 2.1$) of the (K_m, $\log P$) plane (Fig. 15). The group of seven short-period stars is located in similar positions in the period–colour or period–magnitude diagrams (Figs 7, 8 and 9). All of these stars showed relatively inferior periodicity: the mean value of θ was ~ 0.43, compared with the mean of $\theta \sim 0.38$ for the stars in group *A*. We obtained periodic variable stars via our selection criteria (Section 5), but we did not strictly eliminate stars whose periodicities were relatively poor. Hence the stars in group *B* were somewhat semi-periodic compared to the stars in group *A* (see Fig. 5).

11.2 The group *B* stars

To examine the *K*-magnitudes of the short-period variable stars, we compared our estimates with *JHK* observations made by the 1.9-m telescope at the South African Astronomical Observatory (SAAO). Star identification, magnitudes and date of observations are listed in the first five columns of Table 3. Mean *K*-magnitudes derived by equation (14) are tabulated in the 6th column. The first three stars of the table are stars (a), (b), and (g) of group *B*, and the last one was probably a non-AGB star ('⊕' in Fig. 15) of group *B* (see Table 1). The differences in *K*-magnitude obtained at the SAAO

Table 3. JHK magnitude from SAAO.

Star	J	H	K	JD-2450000	$\langle K_m \rangle$	δR_m
nlmc1-324832	12.18	11.12	10.80	2037.3	10.47	0.68
nlmc1-239264	–	12.25	11.83	2037.3	10.81	1.38
nlmc2-19377	12.43	11.36	10.96	2037.3	10.90	0.73
nlmc3-214266	11.74	10.92	10.75	2037.3	10.71	0.71

Note: J, H, K magnitudes are measured to within ± 0.03 mag.

and derived averaged K-magnitude, $\langle K_m \rangle$, were 0.33, greater than 1.02, 0.06, and 0.04, respectively. Except for the second star, nlmc1-239264, the differences do not seem remarkable. We predicted successive light maxima of these four stars using the observed light curves, and have found that the SAAO observations were done near a predicted light maximum for the star nlmc1-324832, and near their predicted light minima for the other three stars. If their light variations were sufficiently regular, the SAAO K-magnitudes of nlmc1-324832 had to be brighter than 10.47. This contradicts the observed brightness, so the regularity of the light variation should be suspected. For the other three stars, K-magnitudes were fainter than their $\langle K_m \rangle$. The observed magnitude for nlmc1-239264 was fainter than our adopted mean magnitude, and the difference was 1.02 mag. Such a difference looked too large when compared with the other two stars. However, the true difference between K_{SAAO} and the mean K would be less than 1.02 mag because the adopted mean magnitude should be brighter than true mean magnitude. Therefore the difference may be acceptable with the true amplitude in R_m greater than 1.38 mag. The question remains as to whether these differences originate from the uncertainty in $\langle K_m \rangle$ or the semi-regular nature of these variables. As indicated in Fig. 14, the K_S magnitudes for seven stars in group B are were located along the line of the O-Miras. This tends to support the use of equation (14) in estimating the K-magnitudes. Further analysis of our data base will resolve this question. Amongst the eight stars of group B, nlmc3-214266 should be a massive star, not a star evolved from the red giant branch or the first red giant branch as pointed out in Section 9.1. We examine the properties of the other seven stars. The differences between the brightness of the group B stars and of the group A stars is evident in Fig. 15. The faintest star, nlmc1-118904, was equally bright in K_S with the other six stars of group B. The amplitude of nlmc1-239264 was larger than the other six stars, but the position on the period-luminosity diagram was not peculiar. We have to study the nature of this star by comparison with more abundant samples to determine whether or not this star is different from the others.

In Fig. 15, the stars in group B were located parallel to the sequence of group A (corresponding to the Mira sequence of Hughes & Wood 1990) and separated by $\delta \log P \sim 0.4$. The seven stars in group B were located at a similar position to the short-period red (SP-red) stars which were reported by Feast & Whitelock (2000) analysing Galactic Miras. While the SP-red stars had large amplitude and Mira-like properties, our group B stars had small amplitudes, except nlmc1-239264, and showed less regular variations, different from the Galactic Miras. The definition of the Galactic Miras is that their amplitude in standard V-light should be larger than 2.5 mag. It is a natural classification because there are few stars with such amplitudes. However, such a gap was not distinct in I-band observations of long-period variables in the LMC (Whitelock 1997). If we try to define Miras in the LMC by Fig. 17, the boundary might be at around 2.2 mag, though the small sample size makes that inconclusive. Therefore we discuss the long-period

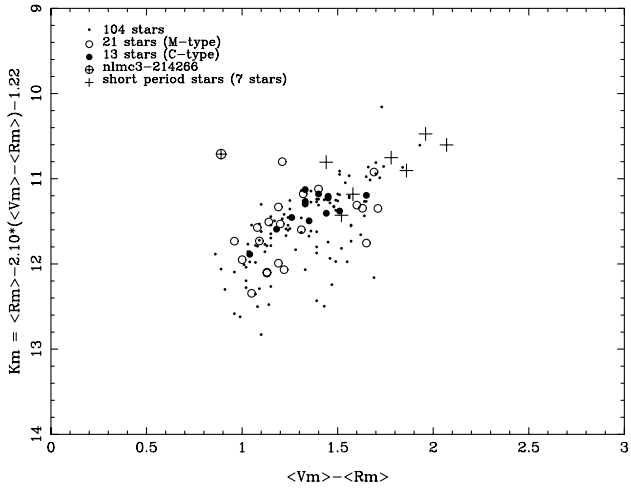

Figure 19. The $(\langle V_m \rangle - \langle R_m \rangle, K_m)$ diagram for 146 samples. The symbols are the same as Fig. 15. The seven stars with short period (+) are located at the reddest and highest luminosity region.

variables of the LMC with no sharp distinction between Miras and semi-regulars.

The theoretical models of long-period variables predict that the ratio of the fundamental to the first or second overtone period should be $\delta \log P \sim 0.3$–0.4. The stars in group B were very similar to those compared with the higher-mode pulsators by Wood & Sebo (1996). Higher-mode pulsators are also expected to have smaller amplitudes than fundamental-mode pulsators. The smallness of the amplitudes of these stars in Figs 17 and 18 supported this point. Therefore, if the stars in group A were fundamental pulsators, the seven stars in group B could be first or second overtone pulsators. On the other hand, as described above, these stars might be the counterparts of SP-red stars reported by Whitelock, Marang & Feast (2000). These authors point out that the kinematics of such stars were different from blue stars with similar periods. Such differences indicate a considerably different stellar age and imply a difference of evolutionary process as a result of a distinct chemical composition. A further development in the theory of stellar structure is needed before it will be possible to judge whether these seven stars are counterparts of SP-red stars (and are higher-mode pulsators) or not.

To study these stars further, we plotted the $\langle V_m \rangle - \langle R_m \rangle$ colour against K_m magnitude in Fig. 19, with the symbols being the same as in Fig. 15. The seven stars of group B are located at the reddest and highest luminosity region where longer-period variables are also located. This suggests that the radius of these stars is very similar to that of longer-period stars. The difference in the period of stars of similar radius is explained by the difference in the mass M and the pulsation property Q. The estimate of the pulsation property for these stars has not been completed because of the uncertainty in the pulsation theory, but the effect of the chemical composition and the stellar mass on Q looks negligible for a given mode (Barthes & Tuchman 1994). The difference in the period–temperature relation found in the globular clusters (Whitelock 1986) has been resolved using different chemical compositions, but the difference in the period of the stars of which the colour is the same cannot be explained this way. The difference in the stellar mass and the mode of pulsation should be studied to explain the difference in the period. When the distribution of periods with stellar physical properties is continuous, it is reasonable to suppose that this is due to changes in stellar mass or other stellar parameters

such as chemical composition. Because the periods of these seven stars are separated from their long-period counterparts, the enhancement of a different mode is suggested. Further progress in data reduction is required to examine the existence of the gap in the periods of this luminous red domain of the colour–K diagram.

When we consider the excitation of different modes, we have to study the reason for such a mode selection. In the classical Cepheids and RR Lyrae stars, the higher-mode pulsators have been found on the blue side, or small stellar radii side, of the colour–magnitude diagram. Therefore it seems difficult to compare the group *B* stars directly with higher mode pulsators of the Cepheid Instability Strip. On the other hand, it may be interesting to compare the surface gravity between them. The surface gravity of the higher-mode pulsators is high for stars in the Cepheid Instability Strip. This implies that the surface gravity of the group *B* stars might be also high. The critical frequency of the stellar atmosphere (i.e. the boundary frequency of reflection or transmission at the stellar surface) must be high for high surface gravity. The enhancement of high frequency, or short-period pulsation in group *B* stars suggests high stellar mass when we suppose the same situation for the transmission and reflection for all pulsating stars.

11.3 The group *C* stars

There are 46 stars in group *C*. Many carbon-rich stars might be included in this group. 12 group *C* stars are the same as the carbon-rich stars tabulated in Hughes & Wood (1990). There was a possibility that about 50 ∼ 60 stars among the sample of 146 are carbon-rich stars as mentioned in Section 10. These carbon-rich stars were estimated to be too faint in our $K_{\rm m}$ conversion. Also, in the amplitude distribution (Fig. 17), there was no obvious difference between group *A* and group *C*. We conclude most group *C* stars were carbon-rich and should be included in group *A*. However, we need to distinguish oxygen-rich stars from carbon-rich stars in order to investigate whether a long-period sequence exists, and if the strip structure is real or not. Future study of the relationship using a *B*-band filter should help resolve this issue.

11.4 Strip structure

Wood (2000) presented the sequential structure of the PL diagram using a large sample. Because our sample size is small, it was hard to confirm this structure, except for the existence of a separate group of red short-period stars. However, it should be noted that these red short-period stars were of small amplitude ($\delta R_{\rm m}$) and less regular (small θ). These will be useful characteristics in the study of the nature of these stars. In the period–K diagram, the stars, nlmc3-214266 and nlmc1-239264, were also contained in group *B*, implying that it is necessary to investigate the properties of individual star even in large-scale photometry in order to understand the period-luminosity relation. The individual star discovered by Wood (2000) should also be checked to determine whether it is to be included in group *B* and the in the set of Galactic red-SP stars.

12 SUMMARY

We selected long-period red LMC variables from the 3-yr MOA data base, and executed a careful period analysis using the PDMM and PDM codes. We selected 146 variable stars using criteria which focus on long-period red variables (Miras and SRs), and investigated their properties. Their observational data were tabulated.

In the ($\log P$,$\langle V_{\rm m}\rangle$) and ($\log P$,$\langle R_{\rm m}\rangle$) diagrams, the luminosity of stars in the major cluster tended to decrease as the period increases. In the ($\log P, \langle V_{\rm m}\rangle - \langle R_{\rm m}\rangle$) diagram, the colours became redder as the periods got longer.

We transformed $V_{\rm m}$, $R_{\rm m}$ magnitudes to $K_{\rm m}$ values using 19 oxygen-rich stars, and presented the period–luminosity (PL) relation in the ($\log P$, $K_{\rm m}$) plane. Many of the stars in our sample, including the large amplitude stars, fell near the position corresponding to the O-Mira sequence by Feast et al. (1989) and Hughes & Wood (1990). A small number of stars (8) formed a separate group in the period–magnitude or period–colour diagrams. This group (group *B*) was found in the bright and short-period region of the ($\log P$, $K_{\rm m}$) plane compared with the O-Mira sequence. These stars showed less periodic variation, and six of them had small amplitudes.

The separation in $\log P$ between the stars and the main group was ∼0.4. They were on the red side of the period–colour diagram and were located at the reddest and brightest tip of the colour–$K_{\rm m}$ diagram similar to the long-period members. If our conversion scale is adequate, it indicates that some of the stars pulsate in a short period compared with the stars which may have a similar radius.

These facts were possibly explained by the assumption proposed by Wood & Sebo (1996): that those six stars with short periods and small amplitudes were higher mode pulsators than the stars on the O-Mira sequence. Two particular stars, nlmc3-214266 and nlmc1-239264, were included in group *B*. These stars showed different features from the other six variable stars. Their pulsation property possibly differs from the other six stars.

In the ($\log P$, $K_{\rm m}$) diagram, below the O-Mira sequence, many stars were located in a wide region. As almost all the identified C-Miras were found in this domain, we supposed that a large number of such variable stars were C-Miras which were more luminous than the magnitude indicated here. In order to reduce the systematic scattering in the ($\log P$, $K_{\rm m}$) diagram, it was necessary to distinguish carbon-rich stars from oxygen-rich stars in advance.

The difficulty in distinguishing oxygen-rich and carbon-rich stars comes from the fact that our blue filter covers both the standard *B* and *V* bands. It is expected that in the future these stars will be observed in the *B* or *V* bands, which will distinguish between carbon-rich and oxygen-rich stars. Alternatively, using any passband which avoids the effect of TiO bands to estimate the bolometric magnitude of the stars could be used. Improvement in the magnitude calibration and confidence in the interpretation of the plural sequences is expected to follow from the analysis of further large observational data bases.

ACKNOWLEDGMENTS

This paper is partly based on DENIS data obtained at the European Southern Observatory. We are grateful to A. Tanaka for his collaboration in preparing the PDM code. We wish to thank P.A.Whitelock for her useful comments and help. We also thank H. Saio for helpful discussions. This work is supported by a grant-in-aid for scientific research (A) of the Japan Ministry of Education, Science, Sports and Culture, and also by the Marsden Fund of the Royal Society of New Zealand.

REFERENCES

Alard C., Lupton R. H., 1998, ApJ, 503, 325
Alcaino G., Liller W., Alvarado F., 1989, A&A, 216, 68
Barthes D., Tuchman Y., 1994, A&A, 289, 429
Becker S. A., 1998, in Bradley P. A., Guzik J. A., eds, ASP Conf. Ser. Vol. 135, A Half Century of Stellar Pulsation Interpretation. Astron. Soc. Pac., San Francisco, p. 12
Bedding T. R., Zijlstra A. A., 1998, ApJ, 506, L47
Caputo F., 1997, MNRAS, 284, 994
Feast M. W., 1996, MNRAS, 278, 11
Feast M. W., 1999, in Le Berte T., Lebre A., Waelkens C., eds, Proc. IAU Symp. No. 191, Asymptotic Giant Branch Stars. Astron. Soc. Pac., San Francisco, p. 109
Feast M. W., Whitelock P. A., 2000, MNRAS, 317, 460
Feast M. W., Glass I. S., Whitelock P. A., Catchpole R. M., 1989, 241, 375
Glass I. S., Feast M. W., 1982, MNRAS, 199, 245
Glass I. S., Lloyd-Evans T., 1981, Nat, 291, 303
Hearnshaw J. B. et al., 2000, in Szadados L., Kuitz D. W., eds, ASP Conf. Ser. Vol. 203, The Impact of Large-Scale Surveys on Pulsating Star Research. Astron. Soc. Pac., San Francisco, p. 31
Holtzman J. A. et al., 1995, PASP, 107, 1065
Hughes S. M. G., Wood P. R., 1990, AJ, 99, 784
Kato Y., 2000, Proc. The Cosmic-Ray Research Section of Nagoya University, Vol. 41. Nagoya Univ., p. 127
Kienzle F., Burki G., Burnet M., Meynet G., 1998, A&A, 337, 779
Kurochkin N. E., 1992, Sov. Astron. Lett., 18, 410
Leavitt H. C., 1908, Harvard Ann., 60, No. 4
Noda S. et al., 2000, in Szadados L., Kuitz D. W., eds, ASP Conf. Ser. Vol. 20, The Impact of Large-Scale Surveys of Pulsating Star Research. Astron. Soc. Pac., San Francisco, p. 80
Schechter P. L., Mateo M., Saha A., 1993, PASP, 105, 1342
Smak J., 1964, ApJS, 9, 141
Stellingwerf R. F., 1978, ApJ, 224, 953
Takeuti M. et al., 2000, in Szadados L., Kuitz D. W., eds, ASP Conf. Ser. Vol. 203, The Impact of Large-Scale Surveys of Pulsating Star Research. Astron. Soc. Pac., San Francisco, p. 120
Trams N. R. et al., 1999, A&A, 346, 843
Yanagisawa T. et al. (MOA Project), 2000, Experimental Astronomy, 10, 519
Walker A. R., 1992, ApJ, 390, 81
Whitelock P. A., 1986, MNRAS, 219, 525
Whitelock P. A., 1999, in Ferlat R., Maillard J.-P., Raban B., eds, Variables Stars and the Astrophysical Returns of the Microlensing Surveys. Editions Frontieres, Gif-sur-Yvette, p. 163
Whitelock P., Marang F., Feast M. W., 2000, MNRAS, 319, 728
Wood P. R., Sebo K. M., 1996, MNRAS, 282, 958
Wood P. R., 2000, Pub. Astron. Soc. Aus., 17, 18

This paper has been typeset from a TEX/LATEX file prepared by the author.